UNIVERSIDADE DO VALE DO RIO DOS SINOS - UNISINOS

Programa de Pós-Graduação em Geologia

Linha de Pesquisa: Estratigrafia e Evolução de Bacias

Seminário Final de Doutorado Acadêmico

Marlise Colling Cassel

ESTUDO TECTONO-SEDIMENTAR DA BACIA DE PELOTAS

São Leopoldo, 25 de março de 2022.

Marlise Colling Cassel

ESTUDO TECTONO-SEDIMENTAR DA BACIA DE PELOTAS

Tese de Doutorado apresentada ao Programa de
Pós-Graduação em Geologia – Área de
Concentração, Geologia Sedimentar Linha de
Pesquisa Estratigrafia e Evolução de Bacias,
da Universidade do Vale do Rio dos
Sinos (UNISINOS), como parte das exigências
para a obtenção do título de Doutora em Geociências

Orientador: Dr. Farid Chemale Jr.

Banca Avaliadora: Dr. Adriano Roessler Viana

Dr. Cleverson Guizan Silva

Dr. Ernesto Luiz Correa Lavina

São Leopoldo, 2022.

C344e Cassel, Marlise Colling.

Estudo tectono-sedimentar da bacia de Pelotas / Marlise Colling Cassel. – 2022.

103 f. : il. ; 30 cm.

Tese (doutorado) – Universidade do Vale do Rio dos Sinos, Programa de Pós-Graduação em geologia, 2022.

“Orientador: Prof. Dr. Farid Chemale Jr.”

Dados Internacionais de Catalogação na Publicação (CIP)

(Bibliotecária: Silvana Dornelles Studzinski – CRB 10/2524)

“It actually doesn’t take much to be considered a difficult woman. That’s why there are so many of us.”

Jane Goodal,

Nactional Geographic

Agradecimentos

Eu agradeço à minha mãe Vera Maria Colling Cassel e meu pai Paulo Henrique Cassel pelo apoio e amor constante, incessante, incondicional e imenso por mais de três décadas.

Eu agradeço ao meu noivo Prof. Dr. Geol. Ezequiel Galvão de Souza pelo amor, companheirismo, presença, afeto, paciência, tolerância, empatia, compreensão dos últimos quase sete anos e em especial durante os anos do doutoramento.

Eu agradeço a todas e todos professores, orientadores e colegas que influenciaram positivamente a minha trajetória de doze anos na Unisinos.

Eu agradeço ao apoio e financiamento da Petrobras, Coordenação para Aperfeiçoamento Pessoal do Nível Superior (CAPES) e Agência Nacional de Petróleo, Gás Natural e Biocombustíveis (ANP).

Agradeço a Linneuniversitetet, Prof. Dr. João Marcelo Medina Ketzer e Lisiane Heemann pela infraestrutura e apoio durante o estágio internacional de pesquisa nos meses finais do doutoramento.

SUMÁRIO

Apresentação

Esta tese foi elaborada na forma de dois manuscritos científicos conforme as normas do Programa de Pós-Graduação em Geologia da Universidade do Vale do Rio dos Sinos (PPGGeo - Unisinos). O trabalho é apresentado através de Resumo e Abstract seguido de quatro capítulos: I. Introdução à Tese, II. Manuscrito 1, III. Manuscrito 2, IV. Síntese Integradora.

O capítulo I, Introdução à Tese, contextualiza o tema desenvolvido ao longo do projeto de doutorado. Este capítulo contém uma introdução geral da bacia, os objetivos, problema central e motivação, bem como os materiais e métodos que conduziram aos resultados. Todos os itens abordados neste capítulo contemplam de forma sucinta o que é apresentado nos manuscritos dos capítulos seguintes.

O capítulo II é composto pelo Manuscrito 1, o qual foi submetido ao periódico científico Global and Planetary Change e está em processo de revisão, sob o título: "*From the Andes and the Drake Passage to the Rio Grande Submarine Fan: paleoclimatic and paleogeographic evidence in the Cenozoic Era from the South Atlantic – Austral Segment, Pelotas Basin*". É um trabalho em escala regional com foco na evolução tectono-sedimentar da Bacia de Pelotas durante o Cenozoico. Neste estudo foi possível diferenciar influências alóctones na Bacia de Pelotas associadas à tectônica da Cordilheira Andina e a mudanças climáticas conectadas à Passagem de Drake durante o Cenozoico. Adicionalmente, estabeleceu-se a interação entre as placas tectônicas Sul Americana, Antártica e Nazca como um agente de controle sobre as influências alóctones supracitadas.

O capítulo III compreende o Manuscrito 2, o qual será submetido ao períodico científico Marine and Petroleum Geology sob o título "*Overpressure modelling in the Rio Grande Submarine Fan, Pelotas Basin: the case study of a gravitational fold and thrust belt in the South*

Atlantic Brazilian Margin”. O objeto central é o Cone de Rio Grande (CRG), uma feição fisiográfica específica da Bacia de Pelotas, com foco na investigação quantitativa, através de modelagem numérica, de sobrepressão. Dentre os resultados, destaca-se a quantificação da sobrepressão na região do CRG, a qual já era especulada na literatura prévia ao explicar o arranjo estrutural complexo decorrente de colapso gravitacional sobre uma superfície de descolamento. Isso implicou em abordar fenômenos divididos como autóctones e alóctones ao sistema: taxa de sedimentação, geração de hidrocarbonetos, tectônica regional e argilominerais.

O capítulo IV trata-se da síntese integradora da tese. Este capítulo contém as principais considerações finais e conclusões obtidas no decurso do projeto de doutorado.

Resumo

A Bacia de Pelotas é a bacia mais a sul da margem brasileira, resultado da ruptura do Gondwana. Possui uma área de cerca de 250.000 km², limitada a norte pelo Alto de Florianópolis (Santa Catarina, Brasil) e a sul pelo Alto Polônio (no Uruguai). A espessura atinge até 12 km do Barremiano ao Recente. É uma bacia singular no Atlântico Sul por fatores como a presença de Seward Dipping Reflectors de grande espessura e, comparada com outras bacias da margem, é ainda considerada depletada em hidrocarbonetos. Por tratar-se de uma bacia com especificidades genéticas (estruturais e estratigráficas), diferente de outras bacias marginais brasileiras, é necessária a geração de novos dados, análise e reinterpretação de dados já existentes. A presente tese de doutorado está comprometida com os aspectos estratigráficos da bacia. Os dois manuscritos apresentados aprofundam os estudos sobre o preenchimento e compartimentação estrutural da bacia. Esta tese utilizou sísmicas e poços da Agência Nacional do Petróleo, Gás Natural e Biocombustíveis (ANP) do Brasil e os softwares Petrel versões 2017, 2018, 2020, desenvolvidos pela Schlumberger e TemisFlow Petroleum System Software versão 2019, desenvolvido pelo Instituto Francês do Petróleo e BeicipFranlab – Consultoria em Óleo e Gás. A tese foi desenvolvida através de interpretação sísmica, backstripping, análise da taxa de espalhamento do Atlântico Sul e modelagem numérica 2D de bacia. Os resultados aqui atingidos identificaram a influência da tectônica da Cordilheira Andina sobre a sedimentação da Bacia de Pelotas na forma de pulsos de soerguimento, bem como a influência climática do alargamento da Passagem de Drake nos depósitos a partir do Oligo-Mioceno através do registro de correntes de contorno. Discriminou-se como raiz destas influências a interação entre as placas tectônicas Sul Americana, Antártica e Nazca. Adicionalmente, foi comprovada de forma inédita existência de sobrepressão no Cone de Rio Grande, bem como identificadas as suas causas como alta taxa de sedimentação, espesso pacote de folhelhos subcompactados e transformação de esmectita em ilita.

Abstract

The Pelotas Basin is the southernmost basin on the Brazilian margin, resulting from the Gondwana breakup. The basin covers an area of 250,000 km², limited to the north by the Alto Florianópolis (Santa Catarina, Brazil) and to the south by the Alto Polonio (Uruguay). Its thickness reaches up to 12 km from the Barremian to the Recent. It is a unique basin in the South Atlantic when compared to other basins of the same margin due to the presence of a very thick package of sewarddipping reflectors and the lack of known hydrocarbon reserves. However, it is still considered hydrocarbons depleted compared to other basins on the margin. Since it is a basin with genetic specificities (structural and stratigraphic), different from other Brazilian marginal basins, it was necessary to generate new data and analyze and reinterpret existing data. The present doctoral thesis is committed to the stratigraphic aspects and comprises studies on the basin filling and structural compartmentalization. The data base includes seismic and wells from the Brazilian National Agency for Petroleum, Natural Gas and Biofuels (ANP). This data was analyzed in the Petrel software versions 2017, 2018, 2020, developed by Schlumberger, and TemisFlow Petroleum System Software version 2019, developed by the French Petroleum Institute and BeicipFranlab – Oil and Gas Consultancy. The studies consisted of seismic interpretation, backstripping, South Atlantic spreading rate analysis, and 2D numerical basin modeling. The results allowed to identify the Andean Cordillera tectonic influence on the Pelotas Basin sedimentation as uplift pulses and identify the climatic influence of the Drake Passage widening from the Oligo-Miocene through the contour currents record. The interaction between the South American, Antarctic, and Nazca tectonic plates was identified as the root of these influences. Additionally, overpressure in the Rio Grande Submarine Fan was well constrained for the first time by numerical modeling, and its causes were identified, including high sedimentation rate, a thick package of subcompacted shales, and smectite-illite transformation.

I. Introdução à Tese

I.1 Caracterização Geral da Bacia de Pelotas

A bacia de Pelotas é uma bacia singular no Atlântico Sul. Um dos fatores é a presença basal de espessas cunhas dominadas por rochas ígneas extrusivas de riftes vulcânicos conectada à Grande Província Ígnea Paraná-Entedeka. Estas cunhas recebem o nome de Seaward Dipping Reflectors (SDR) (Fontana, 1996, Stica et al., 2014). Se comparada a outras bacias marginais brasileiras a Bacia de Pelotas até o momento é depletada em hidrocarbonetos líquidos (Bueno et al., 2007). No entanto há indícios especulativos de outros potenciais sistemas petrolíferos convencionais e fontes não convencionais de hidrocarbonetos para a Bacia de Pelotas. É o caso de folhelhos organógenos turonianos e paleocênicos que se apresentam como potencial rocha geradora da bacia, além dos horizontes de hidrato de gás (Rosa, 2007).

A Bacia de Pelotas é a bacia mais a sul da margem brasileira, com uma área de cerca de 250.000 km^2, limitada ao norte pelo Alto de Florianópolis (Santa Catarina, Brasil) e ao sul pelo Alto Polônio (no Uruguai) (Stica et al., 2014) (Fig. 1). Assim como a Margem passiva da América do sul, é uma bacia originada pela ruptura do Gondwana. Sua espessura atinge até 12 km do Barremiano ao Recente (Fig. 2).

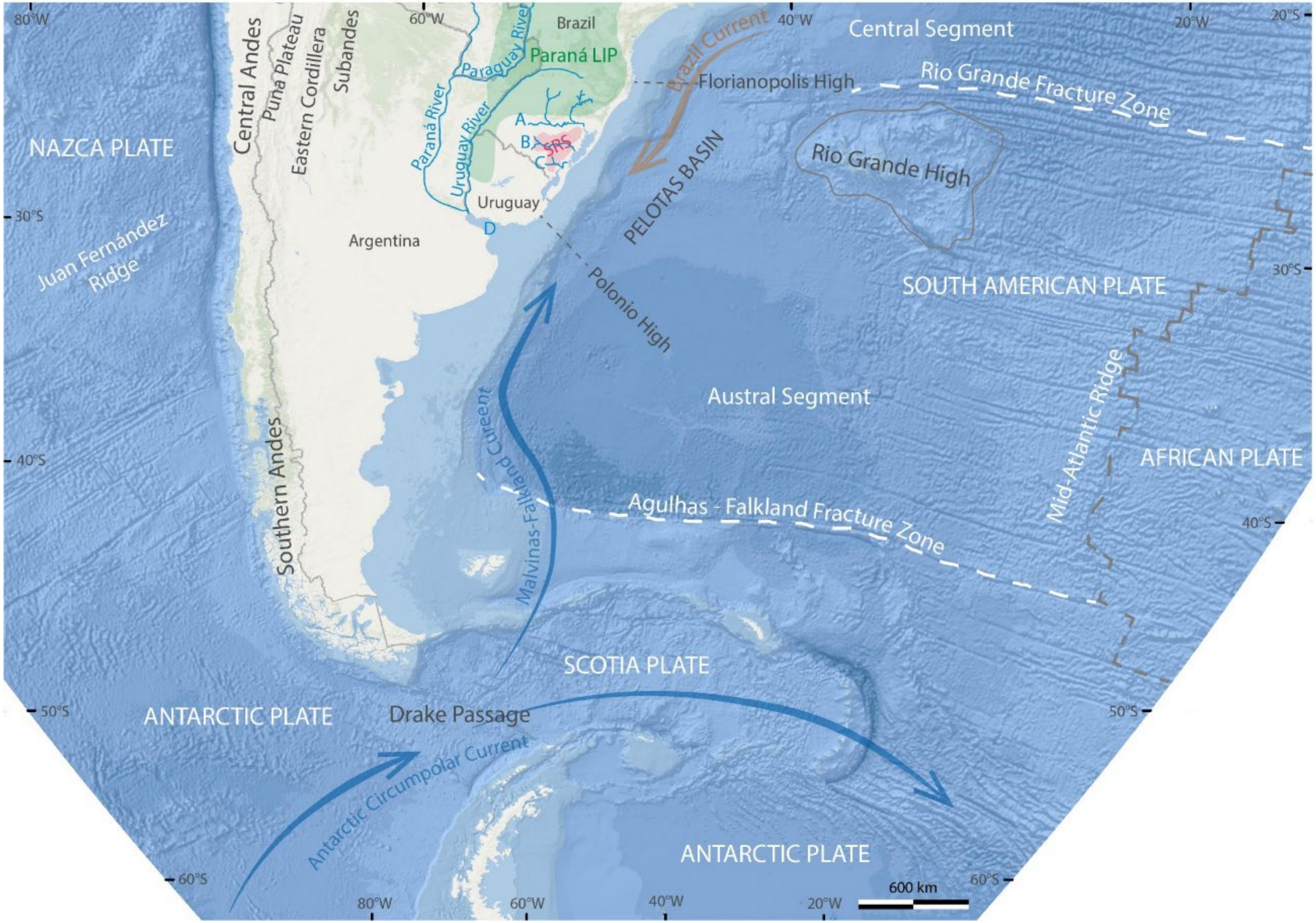
80°W
60°W
40°W
20°W
20°S
Central Andes
Puna Plateau
Eastern Cordillera
Subandes
Brazil
Paraguay River
Paraná LIP
Paraná River
Uruguay River
A
B
SRS
C
Uruguay
D
Argentina
Brazil Current
Florianopolis High
Central Segment
Rio Grande Fracture Zone
Rio Grande High
PELOTAS BASIN
NAZCA PLATE
30°S
Juan Fernández Ridge
Polonio High
SOUTH AMERICAN PLATE
30°S
Austral Segment
Malvinas-Falkland Current
Mid-Atlantic Ridge
AFRICAN PLATE
40°S
Southern Andes
Agulhas - Falkland Fracture Zone
40°S
SCOTIA PLATE
50°S
ANTARCTIC PLATE
Drake Passage
50°S
Antarctic Circumpolar Current
ANTARCTIC PLATE
60°S
80°W
60°W
40°W
20°W
600 km
60°S

Figura 1. Esta figura compõe o Manuscrito 1, como “Figure 1. Map of southern South America showing the main structures on land and in the southern Atlantic Ocean and the location of the Pelotas Basin with its northern and southern limits. Areas: SRS = Sul-Riograndense Shield; Rivers: A = Jacuí; B = Camaquã; C = Piratini; D = Rio de la Plata. Fracture zones and sub-basins according to Stica et al. (2014) and Serrat (2021). Ocean currents according to Stramma and England (1999), Laprida et al. (2011) and Santos et al. (2017).”

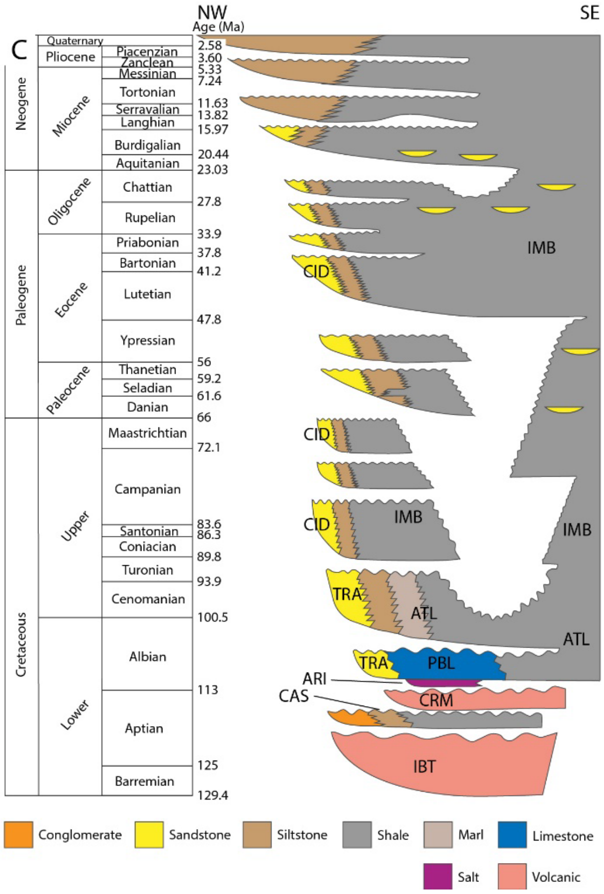

Figura 2. Esta figura compõe o Manuscrito 2, como “Figure 1C) Chronostratigraphic chart of the Pelotas Basin adapted from Bueno et al. (2007). Formations: IBT = Imbituba, CAS = Cassino, CRM = Curumim, ARI = Ariri, PBL = Porto Belo, TRA = Tramandaí, ATL = Atlântida, CID = Cidreira, IMB = Imbé.

O preenchimento da bacia começa quando lavas basálticas subaéreas cobrem o embasamento de crosta continental estendida, os SDR (Abreu, 1998). A sedimentação inicial da bacia ocorre na fase sin-rifte que cobre os SDR. Esta fase consiste em associações de fácies aluviais e lacustrinas compostas por conglomerados, arenitos e siltitos interacamadados. Acima deste pacote, ocorrem cunhas resultantes de extrusões vulcânicas submarinas, que consistem em uma segunda fase de SDR (Abreu, 1998, Bueno et al, 2007) (Fig. 2).

A fase drifte inicia na transição entre Aptiano e Albiano e se estende até o presente (Fontana, 1996). O registro Cenozoico da Bacia de Pelotas é composto por depósitos de ambiente costeiros dominados por leques clásticos que gradam distalmente para folhelhos e siltitos marinhos. A partir do Oligoceno-Mioceno são registrados leques clásticos progradantes sobre depósitos distais, que consiste e uma grande cunha sedimentar regressiva no formada Neógeno. Neste contexto de aumento do aporte sedimentar é registrada a formação de uma feição conhecida como Cone de Rio Grande, ou Leque Submarino de Rio Grande, a qual ainda possui em discussão aspectos referentes a sua gênese. (Abreu, 1998, Bueno et al., 2007, Rosa, 2007, Chemale et al, 2021).

I.1.1 Localização e Compartimentação Tectônica

A costa leste da América do Sul é uma margem passiva, originada pela ruptura do Gondwana. Regionalmente é dividida em três segmentos separados por zonas de fraturaoceânicas: Equatorial, Central e Austral (Fig. 1). A Bacia de Pelotas pertence ao segmento Austral, o qual é limitado a sul pela Zona de Fratura Agulhas-Falkland e a norte pela Zona de Fraturade Rio Grande (ou Florianópolis) (Fontana, 1996; Anjos-Zerfass, 2009).

No extremo norte do segmento Austral, a Bacia de Pelotas, compreende uma área de 250.000 km2. Destes, uma parte emersa de 40.000 km2 constitui a planície costeira do Rio Grande do Sul (Anjos-Zerfass, 2009). É limitada pela Zona de Fraturas de Rio Grande (Fig. 1), que a separa das bacias vizinhas pertencentes ao segmento Central (Bacias de Santos, Campos e Espírito Santo). Na altura do limite norte da bacia dobras simétricas evidenciam uma ampla zona de transcorrência que atingiu partes profundas da bacia, inclusive seu embasamento (Fontana, 1996). Já o limite sul é com o Alto de Polônio, que a separa da Bacia de Punta del Este. O limite oeste, na porção onshore, ocorrem espessos pacotes de lava pertencentes à Formação Serra Geral (Cretáceo da Bacia do Paraná) que integram a Província Ígnea Paraná-Etendeka (Stica et al., 2014).

Esta grande província ígnea e sua correlata na Namíbia, somadas às cunhas de seaward-dipping reflectors (SDR) nas margens da América do Sul e da África constituem a Província Ígnea do Atlântico Sul (Stica et al., 2014). Os SDR são refletores superpostos, acunhados, que mergulham para o oceano, sem ter uma aparente terminação basal e são localmente convexos para a superfície. A testemunhagem e análises geoquímicas deste intervalo indicaram basaltos toleíticos extrudidos em condições subaéreas, com composição no campo de transição entre basaltos oceânicos e continentais (Fontana, 1996). A composição destes basaltos é mutável no sentido da crosta continental para a oceânica, conforme aumenta o grau de estiramento da crosta. Estão associados aos instantes iniciais do rifteamento e representam a anomalia magnética mais antiga e mais próxima da costa sul brasileira. A espacialização desta feição se superpõe à anomalia G de Rabinowitz e La Brecque (1979), previamente traçada e previamente interpretada como limite da crosta continental e oceânica. Porém interpretações mais recentes postulam o contato entre crosta continental e oceânica sobre as anomalias M0 e M3 (Fontana, 1996).

A Bacia de Pelotas, instalada por sobre crosta continental e oceânica, tem como estruturas principais estratos mergulhando suavemente em direção ao oceano. Estes estratos formam uma cunha que recobre o embasamento cortado por falhas antitéticas de grande rejeito, formando hemi-grabens assimétricos e falhas sintéticas de pequeno rejeito (Fontana, 1996; Abreu, 1998; Rosa, 2007; Stica et al., 2014). Na região do Cone de Rio Grande o que chama a atenção é a implantação de falhas normais conjugadas com falhas de compensação de origem adiastrófica (Rosa, 2007).

I.1.2 Preenchimento

Há diferenças marcantes de preenchimento entre as bacias da margem sul e sudeste, principalmente no que diz respeito à deposição de sal e presença de hidrocarbonetos. As bacias do segmento Austral constituem um sistema de rifte, vulcânicos, com grande volume de cunhas de SDR, e sem a deposição de sal. Enquanto que o segmento Central é empobrecido na atividade magmática, possui exumação do manto e espessos pacotes de sal (Stica et al., 2014). Tal fenômeno ocorre devido à barreira geográfica exercida pelo Alto de São Paulo e Plataforma de Florianópolis durante o Aptiano. Esta feição limitou a livre circulação marinha, ocasionando uma restriçãoambiental e formação de evaporitos na Bacia de Santos. Por outro lado, na Bacia de Pelotas, a livre circulação acarretou em sedimentação francamente marinha (Fontana, 1996; Abreu, 1998; Anjos-Zerfass, 2009; Stica et al., 2014).

O preenchimento da Bacia de Pelotas evolui em fases distintas, tal como na margem sul africana: Megassequencia Pré Rifte, Megassequencia Rifte, Cunha Passiva (Estágio Inicial e Final) (Fontana, 1996), a qual é equivalente a Fase Pós Rifte e Drifte (Bueno et al., 2007 Abreu, 1998). A fase Drifte é dividida, segundo Abreu (1998) em Transgressiva, Agradacional e Regressiva, e segundo Bueno et al. (2007) em Plataformal, Transgressiva e Regressiva.

O pacote Pré Rifte é o embasamento da Bacia de Pelotas, composto por rochas do embasamento cristalino do Escudo Sul-Riograndense na metade sul da Bacia. Enquanto que na metade norte da bacia o embasamento é composto pela Bacia do Paraná (Fontana, 1996; Bueno et al., 2007). O pacote Rifte é composto pela fase de deposição aluvial e lacustre com comglomerados e siltitos intercalados da Fomação Cassino. Após este pacote ocorre a formação das SDR´s, cuja nomenclatura litoestratigráfica refere-a como Formação Curumin (Abreu, 1998; Bueno et al., 2007).

Na transição Aptiano-Albiano tem início a Fase Drifte (ou Cunha Passiva Inicial) (Fontana, 1996). Este fase da bacia representa um período transgressivo de larga escala, do Albiano ao Oligoceno. Inicialmente é classificada por Bueno et al. (2007) como Drifte Plataformal, e por Abreu (1998) como Drifte Transgressivo. Inicia com a Formação Ariri, restrita a uma pequena extensão no norte da Bacia, próximo ao limite com a Bacia de Santos. Trata-se de delgados evaporitos interdigitados com carbonatos. O contato superior é concordante com a Formação Tramandaí, a qual migra lateralmente para a Formação Porto Belo. Estas formações consistem em depósitos de uma plataforma mista composta por arenitos finos de marinho raso (Fm. Tramandaí), que configura a porção mais proximal, a qual grada para carbonatos bioclásticos e calcarenitos oolíticos a calcilutitos (Fm. Porto Belo) (Abreu, 1998; Bueno et al. 2007).

A tendência transgressiva geral do Drifte que a bacia segue faz com que esta relação lateral de fácies descrita anteriormente mude, de forma parcialmente discordante, suprimindo as fácies carbonáticas da Formação Porto Belo. Tem início, segundo Bueno et al. (2007), a Fase Dirfte Transgressivo, no meio do Albiano. Desta Forma o marinho raso da Formação Tramandaí migra lateralmente para a configuração mais distal da plataforma caracterizada por sedimentação fina silicilástica e mista, na forma de siltitos e margas da Formação Atlântida, a qual tem contato inferior discordante sobre a Formação Porto Belo (Abreu, 1998; Bueno et al., 2007).

A partir do Turoniano a tendência transgressiva fica efêmera na bacia, ocorrendo também erosões acentuadas, intercaladas a estes eventos transgressivos (Fontana, 1996; Abreu, 1998; Bueno et al., 2007). Isso, segundo Abreu (1998) marca o início da fase Drifte Agradacional. Destes eventos, de mais ampla distribuição ocorre no Paleoceno. Este padrão efêmero segue até o Oligoceno (Oligoceno inicial para Abreu (1998) e Oligoceno Final para Bueno et al. (2007)). O ambiente costeiro passa a ser dominado pelos leques clásticos grossos e finos da Formação Cidreira que migram lateralmente para folhelhos e siltitos de ambiente marinho profundo, com depósitos turbidíticos da Formação Imbé. Estas duas Formações seguem na bacia até o Holoceno.

No Oligoceno inicia a fase Drifte Regressiva. Nesta fase ocorre a progradação dos leques clásticos e deltas progradantes da Formação Cidreira por sobre os depósitos distais da Formação Imbé. Esta tendência ocorre na maioria das bacias da margem brasileira, caracterizando uma grande cunha sedimentar regressiva no Neógeno. Neste contexto de aumento no aporte sedimentar que ocorre a formação do Cone de Rio Grande (Abreu, 1998; Bueno et al., 2007).

I.2 Problema e Motivação da Tese

Por tratar-se de uma bacia com especificidades genéticas (estruturais e estratigráficas), diferente de outras bacias marginais brasileiras, é necessária a geração de novos dados, bem como a análise e reinterpretação de dados já existentes. Estes dados devem servir: a) à compreensão da herança estrutural do embasamento nas diferentes porções da bacia na fase de abertura do Atlântico, b) ao entendimento da evolução tectono-sedimentar das bacias de margens passivas conjugadas na África do Sul (bacias Luderitz, Walvis Ridge e Orange) e margem brasileira (Bacia de Pelotas), c) e ao detalhamento do seu preenchimento sedimentar e de estruturas geradas durante as fases de fragmentação e deriva dos continentes e por fim d) desvincular pressupostos conceituais herdados de outras bacias marginais. A presente tese de doutorado está comprometida com os aspectos estratigráficos da bacia, aprofundando os estudos sobre o preenchimento e compartimentação estrutural.

I.3 Objetivos

O estudo tectono-sedimentar da Bacia de Pelotas objetivou: entender os controles regionais e suas implicações na deposição da bacia. Este objetivo geral está presente nos dois manuscritos da tese, na forma de diferentes objetivos específicos, abordados nos respectivos manuscritos dos capítulos seguintes.

O Manuscrito 1 objetivou a identificação e entendimento de controles tectônicos regionais alóctones à Bacia de Pelotas e como é seu registro na bacia. O Manuscrito 2, aplicando parte dos resultados do Manuscrito 1, ao seguir um fluxo de trabalho de escala regional para local, objetivou investigar quantitativamente ocorrência de sobrepressão no Cone de Rio Grande.

I.4 Materiais e Métodos

Ao longo dos quatro anos do desenvolvimento da tese os materiais utilizados foram dados de exploração obtidos com a Agência Nacional do Petróleo, Gás Natural e Biocombustíveis (ANP) do Brasil. Trata-se de seções sísmicas e dados de poços da Bacia de Pelotas (Fig). A localização. Esta base de dados foi analizada nos softwares Petrel versões 2017, 2018, 2020, desenvolvidos pela Schlumberger e TemisFlow Petroleum System Software versão 2019, desenvolvido pelo Instituto do Petróleo e BeicipFranlab – Consultoria em Óleo e Gás.

As técnicas utilizadas variaram conforme o manuscrito e tais aspectos são aprofundados em cada um deles nos respectivos capítulos. Os subitens a seguir esclarecem aspectos introdutórios da metodologia, posteriormente abordados em cada manuscrito. O Manuscrito 1 envolve backstripping, análise da taxa de espalhamento do Atlântico Sul e interpretação sísmica. O Manuscrito 2 aborda conversão tempo-profundidade de seção sísmica e modelagem numérica 2D de bacia.

I.4.1 Aplicados no Manuscrito 1

A figura abaixo (Fig. 3), ilustra o fluxo de trabalho adotado no manuscrito 1. Os dados extraídos do modelo de backstripping foram comparados com os dados de taxa de espalhamento do Atlantico Sul. Esta comparação permitiu a identificação de padrões cronocoerraltos, os quais foram melhor compreendidos através de associação com eventos da geologia regional e posteriormente mapeados nas seções sísmicas. Cada uma destas etapas mencionada aqui e visualizada no fluxograma abaixo é detalhada nos subitens a seguir.

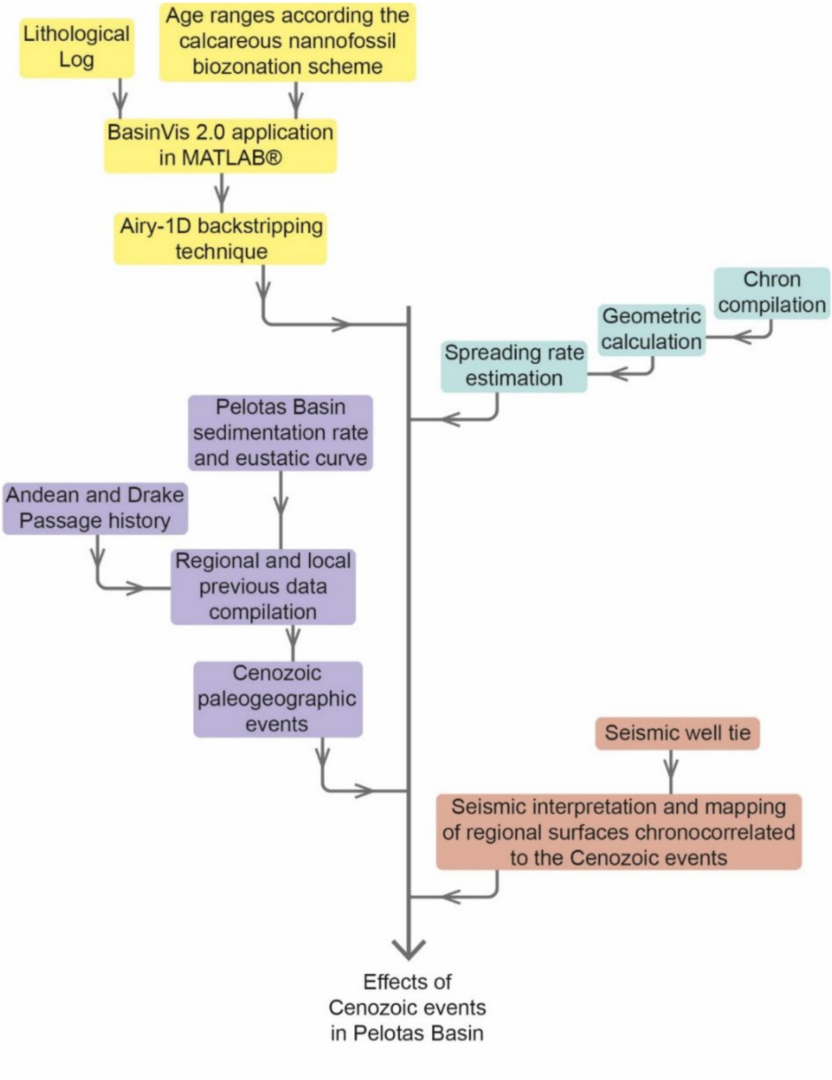

Figura 3. Esta figura compõe o Manuscrito 1, como "Figure 3. Methodological workflow applied in the identify the effects of Cenozoic events in Pelotas Basin."

I.4.1.1 Backstripping

Para gerar as curvas do modelo de backstripping escolhemos quarto poços na bacia de pelotas e usamos o aplicativo BasinVis 2.0 no MATLAB® (Lee e Wagreich, 2018). Os poços estão identificados e podem ser visualizados na Figura 4. Estes poços foram escolhidos devido a necessidade de controle bioestratigráfico. Neste caso, como o artigo tratou do intervalo Cenozoico adotamos o esquema bioestratigráfico de Gomide (1989) com nanofosseis calcários.

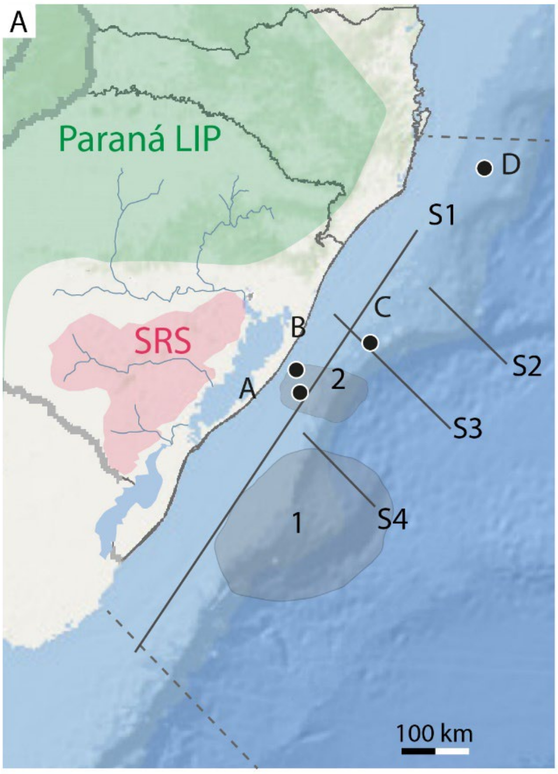

Figura 4. Esta figura compõe o Manuscrito 1, como "Figure 2. A) Map of the Pelotas Basin with interpreted seismic sections and wells. Seismic sections: S1 = 0034-0005, S2 = 0231-1349, S3 = 0228-0317, S4 = 0277J99B342. Wells: A = 1-RSS2-RS, B = 1-RSS3-RS, C = 2-RSS1-RS, D = 1-SCS2-SC. SRS = Sul-Riograndense Shield; 1 = Rio Grande Submarine Fan; 2 = Mostardas Low. "

Pela remoção gradual de sinais eustáticos, sedimentares e de carregamento de água para pacotes individuais de preenchimento de bacia datados, a técnica isola um histórico de profundidade da bacia que é interpretável em termos de elevação e subsidência de controles tectônicos (Lee et al., 2019). O intervalos de tempo estão de acordo com o esquema de biozonação de nanofósseis calcários de Gomide (1989). Para fins práticos, o embasamento foi considerado qualquer biozona correspondente a N340 ou mais antiga (Material Suplementar SM1 – Biozonação). A paleobatimetria foi baseada nos valores apresentados por Koutsoukos (1982). Para a curva eustática, foram utilizados os valores de Abreu e Anderson (1998).

O modelo tectônico compensado 1D (Z) para qualquer tempo geológico t, é assim obtido com

$$Z(t) = S(t).\left(\frac{\rho_m+\rho_s}{\rho_m-\rho_w}\right) + W_d(t) - \Delta_{SL}(t).\left(\frac{\rho_m}{\rho_m-\rho_w}\right)$$

onde S(t) refere-se à profundidade da camada de sedimento descompactado em qualquer tempo (t), and ρ_m, ρ_s and ρ_w são as densidades médias do manto (3300 kg/m3), sedimentos (2300 kg/m3) e água (1000 kg/m3), respectivamente. $W_d(t)$ refere-se à paleobatimetria no tempo t, and Δ_{SL} a mudança do nível do mar eustático entre o tempo te o presente (Lee et al., 2019).

I.4.1.2 Análise da Taxa de Espalhamento do Atlântico Sul

O cálculo da taxa de espalhamento do Atlântico Sul foi estimado para as latitudes compreendidas dentro dos limites da Bacia de Pelotas. Para melhorar a confiabilidade de nossos dados, medimos ao longo de três trilhas diferentes entre pares das principais zonas de fratura: (I) as zonas de fratura de Tristão da Cunha e Chui; (II) as zonas de fratura de Chui e Porto Alegre; e (III) as zonas de fratura de Porto Alegre e Rio Grande, que atravessam o setor da

Bacia de Pelotas. A taxa de espalhamento foi então estimada a partir dos valores médios determinados a partir dos espaçamentos isócronos entre os três pares de zonas de fratura.

As variações da taxa de espalhamento do fundo do mar podem ser estimadas a partir dos espaçamentos das isócronas de reversão magnética em perfis individuais de trilhas de navios (Pérez-Díaz et al., 2020). Para calcular a taxa de espalhamento na Dorsal Meso-Oceânica do Atlântico Sul (SAMOR) na latitude da Bacia de Pelotas, utilizamos o conjunto de dados compilado por Seton et al. (2014) a partir das isócronas de Cande et al (1988), Müller et al (2008) e Pérez-Díaz e Eagles (2014). O intervalo estudado refere-se ao período de acreção crustal oceânica entre chron C27n (60,92 Ma; Gee e Kent, 2007) e o presente. Este intervalo exclui o efeito de saltos relacionados à elevação do Rio Grande (Pérez-Díaz e Eagles et al., 2017). Devido à pequena mudança na posição e geometria do SAMOR desde 60 Ma (ancorado ao eixo de rotação – Müller et al., 2016), podemos definir com segurança a taxa de espalhamento com base na taxa entre intervalo de tempo versus espaçamento de isócronas de reversão no oeste lado de SAMOR.

I.4.1.3 Interpretação Sísmica

As seções símicias utilizadas no manuscrito 1 estão identificadas e podem ser visualizadas na figura Figura 3. Foram escolhidas seções que abrangessem regionalmente a área da bacia, de forma amplamente disctribuida, e que estivessem próximas de poços específicos.

A proximidade com os poços específicos foi um dos critérios devido a necessidade de controle bioestratigráfico. Neste caso, como o artigo tratou do intervalo Cenozoico adotamos o esquema bioestratigráfico de Gomide (1989) com nanofosseis calcários para poços da Bacia de Pelotas. Cada evento identificado a partir das técnicas descritas nos subitens anteriores (Backstripping e Análise da Taxa de Espalhamento do Atlântico Sul) foi localizado em tempo no poço devido ao controle de idades que a bioestratigrafia de nanofosseis calcários de Gomide (1989) fornece. A partir do poço intersectado com uma seção sísmica o refletor correspondente à idade de interesse foi rastreado para o restante das seções sísmicas. Assim que identificado e mapeado nas seções sísmicas, o refletor de interesse foi descrito.

I.4.2 Aplicados no Manuscrito 2

Para o Manuscrito 2 utilizou-se seção sísmica e poço localizados no Cone de Rio Grande (Fig. 5). A escolha da linha ocorreu devido a presença de arcabouço estratigráfico com resolução de interpretação de refletores adequada elaborada por Rosa (2007) (Fig. 6). Trata-se de uma seção dip NW-SE de 160300 m de comprimento e 11000 ms em templo duplo de percurso.

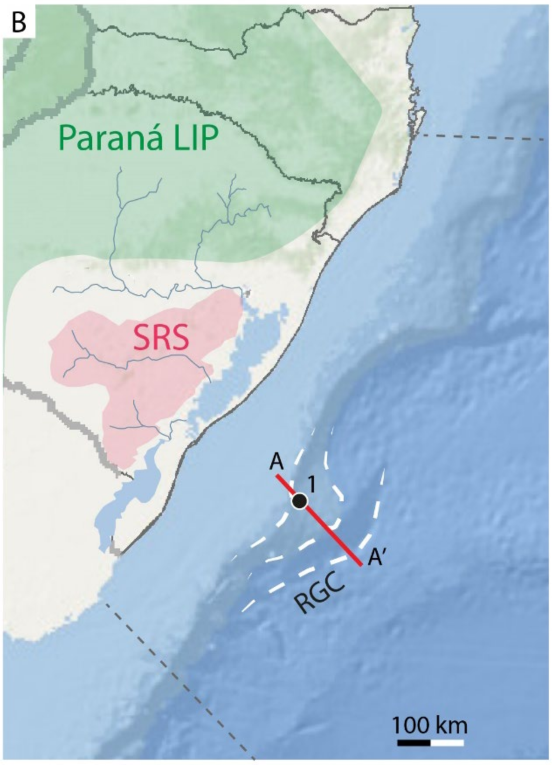

Figura 5. Esta figura compõe o Manuscrito 2, como “Figure 1. B) Map of the Pelotas Basin with interpreted seismic section (A-A’ = J99B194) and well (1 = 1BRSA61RSS).”

A escolha do poço levou em conta sua proximidade com a seção sismica. Os dados do poço são aplicados na conversão tempo-profundidade dos horizontes interpretados da seção sísmica. Esta etapa requer que o poço e a seção sísmica se intersectem.

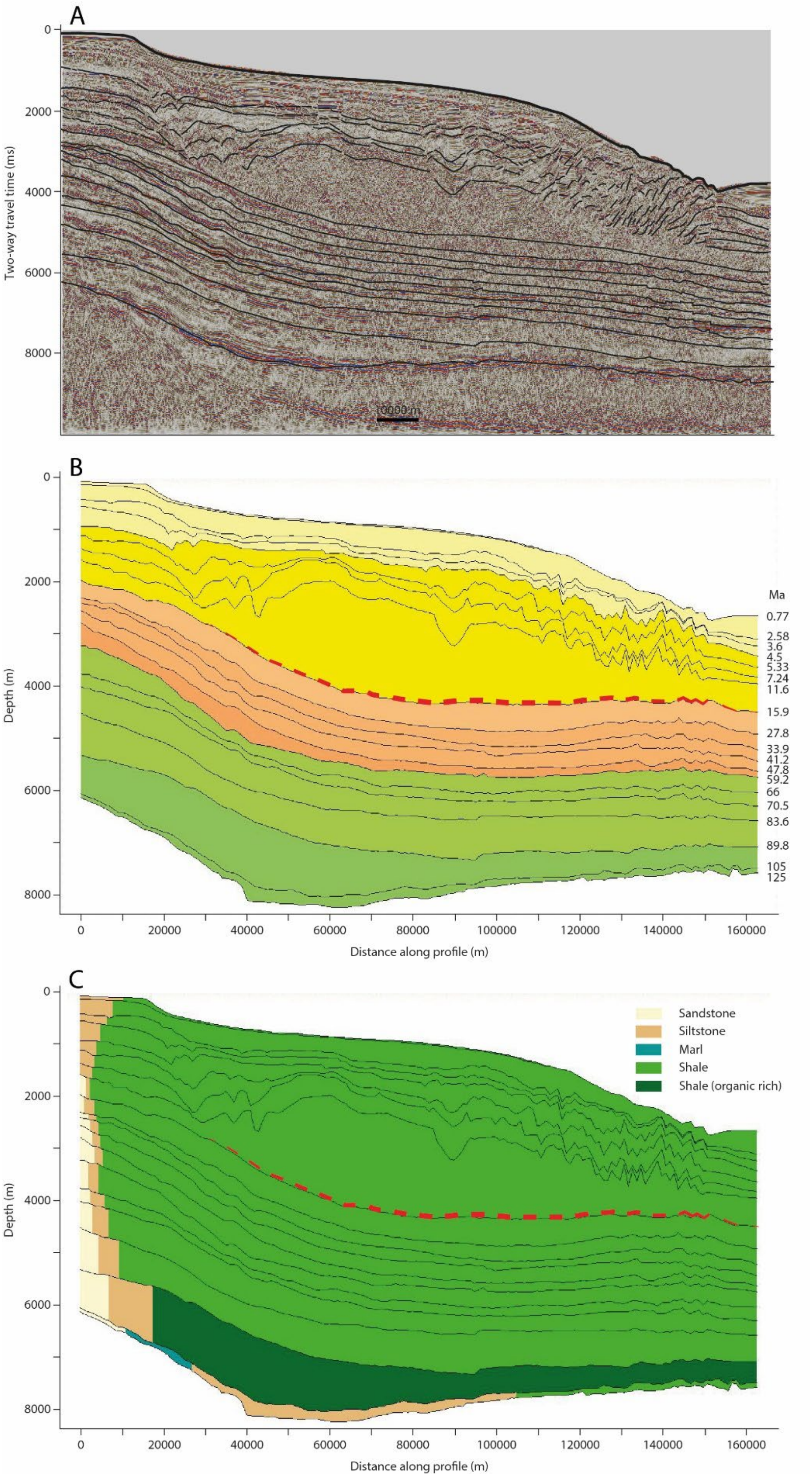

Figura 6. Esta figura compõe o Manuscrito 2, como “Figure 2. A) Interpreted seismic line in two-way time, where the colored lines indicate stratigraphic surfaces described in Rosa (2007) and the red-black dashed line indicates the RGF basal detachment surface, modified from Rosa (2007). Above the basal surface, the RGF displays different structural domains, where the proximal portion corresponds to distensive listric faults. In contrast, the distal portion corresponds to compressive gravitational fold and thrust belt. B) The stratigraphic framework (according to Rosa, 2007), in depth, highlighting the detachment surface in the red dashed line. C) Main lithologies (according to Bueno et al., 2007), in depth, highligting the detachment surface in the red dashed line.”

1.4.2.1 Conversão tempo-profundidade

A conversão tempo-profundidade dos horizontes sísmicos interpretados considerou a equação do tempo de viagem da onda sísmica refletida verticalmente (Equação 1):

Profundidade = (velocidade média) × (tempo duplo/2)

Onde o tempo duplo é o tempo do horizonte interpretado na seção *zero-offset* e a velocidade média é o perfil de velocidade obtido do perfil sísmico vertical do Poço 1 (VSP).

1.4.2.2 Modelagem numérica 2D de bacia

A modelagem 2D da bacia foi executada no software TemisFlow Petroleum System (IFPen – French Institute of Petroleum, versão 2019). O primeiro passo foi importar os horizontes (anteriormente convertidos em profundidade). Posteriormente, cada horizonte recebeu uma idade, seguindo o quadro estratigráfico de Rosa (2007) (Fig. 6). Em seguida, cada intervalo entre os horizontes recebeu litologias, segundo Bueno et al. (2007) e Rosa (2007) (Fig. 6).

Para modelagem de sobrepressão, foram computadas variáveis como porosidade, permeabilidade e taxa de sedimentação. As variáveis de porosidade e permeabilidade utilizadas nesta modelagem foram extraídas da Biblioteca de Litologia do IFPen e a variável taxa de sedimentação foi calculada restaurando geometrias passadas. O TemisFlow realiza esta função através da técnica de backstripping baseada na geometria atual e nas leis de compactação de litofácies.

O próximo passo foi parametrizar as condições de temperatura. A computação da distribuição de temperatura resultante da transferência de calor através da bacia sedimentar requer a definição de um embasamento térmico. As opções disponíveis no TemisFlow para cálculo de regimes térmicos incluem gradientes geotérmicos, fluxo de calor nos sedimentos de base, fluxo de calor na base do manto superior. Com base nos dados de poços disponíveis, o modelo foi rodado com 20°C/km como gradiente térmico e temperatura do fundo do mar variando de 6°C (águas rasas) a 3°C (águas profundas a 13600 m), de acordo com Ketzer et al. (2020).

II. Manuscrito 1

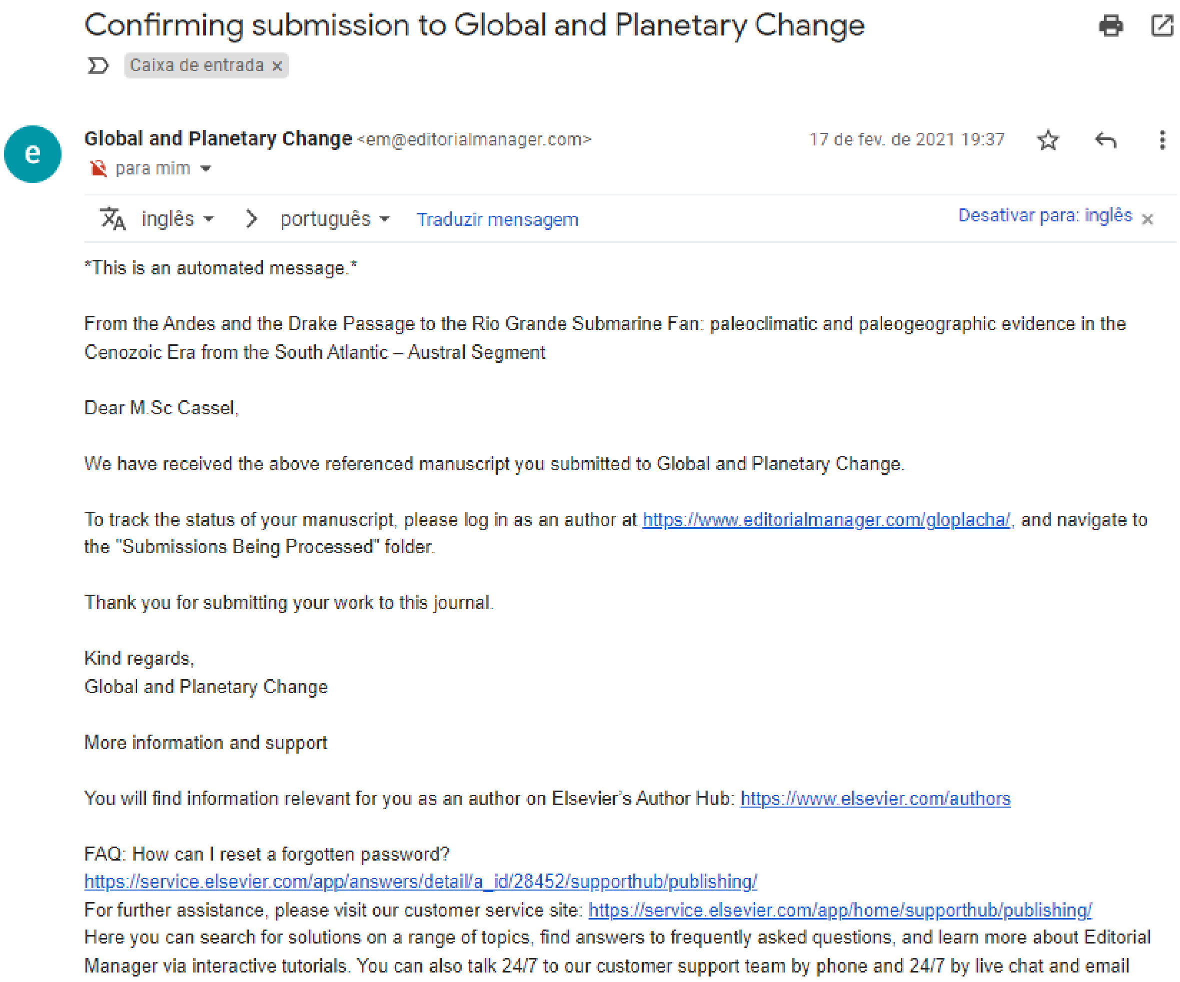

Confirming submission to Global and Planetary Change

Global and Planetary Change <em@editorialmanager.com>

17 de fev. de 2021 19:37

This is an automated message.

From the Andes and the Drake Passage to the Rio Grande Submarine Fan: paleoclimatic and paleogeographic evidence in the Cenozoic Era from the South Atlantic – Austral Segment

Dear M.Sc Cassel,

We have received the above referenced manuscript you submitted to Global and Planetary Change.

To track the status of your manuscript, please log in as an author at https://www.editorialmanager.com/gloplacha/, and navigate to the "Submissions Being Processed" folder.

Thank you for submitting your work to this journal.

Kind regards,
Global and Planetary Change

More information and support

You will find information relevant for you as an author on Elsevier's Author Hub: https://www.elsevier.com/authors

FAQ: How can I reset a forgotten password?
https://service.elsevier.com/app/answers/detail/a_id/28452/supporthub/publishing/
For further assistance, please visit our customer service site: https://service.elsevier.com/app/home/supporthub/publishing/
Here you can search for solutions on a range of topics, find answers to frequently asked questions, and learn more about Editorial Manager via interactive tutorials. You can also talk 24/7 to our customer support team by phone and 24/7 by live chat and email

From the Andes and the Drake Passage to the Rio Grande Submarine Fan: paleoclimatic and paleogeographic evidence in the Cenozoic Era from the South Atlantic – Austral Segment, Pelotas Basin

Marlise Colling Cassel*[1], Farid Chemale Jr. [1], Mateus Rodrigues Vargas[1], Marcelo Kehl de Souza[1], Tiago Jonatan Girelli[1], Gisela Serêjo de Oliveira [1]

[1]Vale do Rio dos Sinos University, Geology Graduate Program, Av. Unisinos, 950, São Leopoldo, Rio Grande do Sul, CEP 93022-000, Brazil

*corresponding author: Marlise Colling Cassel (marlise.cassel@gmail.com)

Abstract

The Cenozoic depositional history of the Pelotas Basin was driven by the interaction between the spreading processes of the Atlantic Ocean and the formation of the Andean Cordillera. We integrated seismic interpretation and backstripping techniques with evaluation of spreading rates in the South Atlantic and subduction beneath the Andes to unveil the main climatic, eustatic and active tectonic events in the Cenozoic. The achieved results integrated with regional geology and Cenozoic history data show the tectonic control that the Andean Cordillera exerted over the Pelotas Basin's passive margin. On the other hand, climatic and glacioeustatic changes that influenced the Pelotas Basin's sedimentation were mostly controlled by the tectonic opening of Drake Passage and the consequent onset of the Antarctic Circumpolar Current. These processes were directly connected to motions of the Antarctic, South American, and Nazca plates since the beginning of the Cenozoic. Our results allow us to detail the geological events of the Pelotas Basin and more accurately define its eustatic, tectonic, and climatic controls by closely observing the interaction between compressive tectonics and passive margins.

Keywords: Passive margin; Compressive tectonics; Glaciotectonic; Antarctic Circumpolar Current; Pelotas Basin; Paleogeography.

1. INTRODUCTION

The Earth has experienced paleogeographic and paleoclimate events in the Cenozoic that contributed substantially to the present-day geological configuration. These events include the opening and closing of oceanic gateways, hyperthermal events, climate transitions, and the rise of mountain chains, providing valuable paleoclimatic comparative constraints for projections of the Earth´s future (Zachos et al., 2008, Potter and Szatmari, 2009, Wright, 2009, Mudelsee et al., 2014). In contrast to the present, much of the eary Cenozoic was characterized by high concentrations of greenhouse gases, high global average temperatures, the absence of ice caps in the poles, and a low-temperature gradient between high and low latitudes. Over the last 34 Ma, the atmospheric CO_2 concentration and global temperature dropped, and a continental ice sheet developed in Antarctica (Zachos et al., 2008, Mudelsee et al., 2014). Along with long-term climate system feedbacks, these changes have also been attributed to the effects of long-term geographic changes on oceanographic and atmospheric circulation patterns (Mudelsee et al., 2014).

During the Cenozoic, the Andean convergence zone has experienced a complex pattern of compressional and extensional events at different latitudes and different times, resulting in a variety of tectonic domains (Horton, 2018). This mixed scenario is the result of differential decoupling along the plate boundary during slab rollback. According to Horton (2018), while a retreating subduction system has tended to dominate the Southern Andes, shallow subduction has maintained strong plate coupling in the Central Andes. These compressional and extensional scenarios resulted in repeated uplift pulses in the Central Andes and the development of extensional domains in the Southern Andes (Canavan et al., 2014, Carrapa et al., 2014, Quade et al., 2014, Horton, 2018). Additionally, at around 50 Ma, a marked increase in the divergence rate between the South American and Antarctic plates led to the widening of the Drake Passage and, in turn, to a gradual increase in interaction between Pacific and Atlantic waters in the Southern Ocean (Livermore et al., 2007). Antarctic glaciation also began intermittently and, by 34 Ma, led to the formation of a continental ice sheet (Zachos et al., 2008). Close to the boundary between the Oligocene and Miocene, Drake Passage had become wide enough to permit intensification and broadening of the Antarctic Circumpolar Current (ACC) (Zachos et al., 2008, Zhang et al., 2013). However, short-lived warming episodes punctuated the accompanying long-term cooling trend, such as the Middle Miocene Climate Optimum (Zachos et al., 2008, Zhang et al., 2013).

Large submarine fans grew throughout the Cenozoic. Starting in the Neogene, there was a six-fold increase in the accumulation of hemipelagic mud (Potter and Szatmari, 2009). Voluminous Neogene submarine fans are registered worldwide, the majority composed of muddy sediments, like the Amazon and Bengal-Nicobar fans (Damuth and Kumar, 1975; Curray et al., 2003, Potter and Szatmari, 2009; McNeil et al., 2017, Horn et al., 2017, Chemale et al., 2021). In the South Atlantic Ocean, the Rio Grande Submarine Fan has accumulated since the Miocene to become the most prominent sedimentary feature in the Pelotas Basin (Rosa, 2007; Castillo-López, 2009; Anjos-Zerfass et al., 2014; Chemale et al., 2021).

In this work, we aim to show how the succession of global and regional tectonic events described above is recorded in the sedimentation history of passive margin basins in the southern portion of the Atlantic Ocean, in particular that of the Rio Grande Submarine Fan. To do this, we carried out a multiproxy analysis using subsurface data and regional information to identify the effects of climatic, eustatic, and tectonic triggers. The analysis requires integration of data on extensional passive margins, compressive Andean orogenic systems, and plate rearrangements to better understand climate changes and the tectono-sedimentary influence in the evolution of the Pelotas Basin.

2. GEOLOGICAL SETTING

The South American passive margin originated during the early Cretaceous breakup of Gondwana. Regionally, it can be divided into three segments separated by oceanic fracture zones: the equatorial, central, and austral segments (Fig. 1). The Pelotas Basin is part of the austral segment, which is bounded to the south by the Agulhas-Falkland Fracture Zone and to the north by the Rio Grande Fracture Zone (Fontana,1996; Stica et al., 2014) (Fig. 1).

Located at the northernmost austral segment, the Pelotas Basin covers 250,000 km², with an emergent part of the basin underlies a coastal plain with an area of 40,000 km² (Anjos-Zerfass, 2009). The Pelotas Basin is limited to the north by the Santos Basin through the Rio Grande Fracture Zone (Fig. 1). The southern limit is within the Polônio High, separating the Pelotas Basin from the Punta del Este Basin (Stica et al., 2014) (Fig. 1).

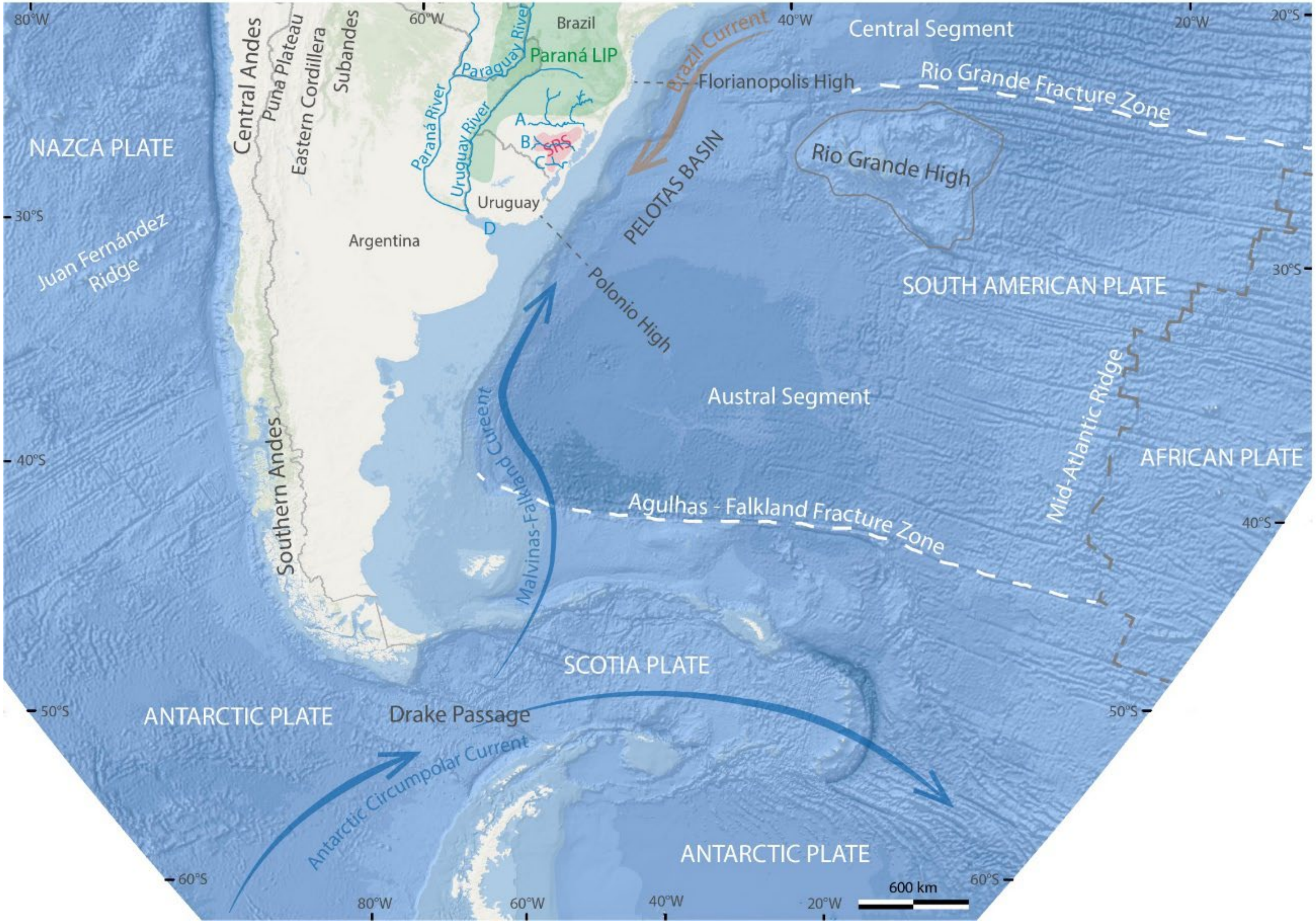
80°W
60°W
Brazil
40°W
Central Segment
20°W
20°S
Central Andes
Puna Plateau
Eastern Cordillera
Subandes
Paraguay River
Paraná LIP
Brazil Current
Florianopolis High
Rio Grande Fracture Zone
Paraná River
Uruguay River
A
B
SRS
C
Rio Grande High
NAZCA PLATE
PELOTAS BASIN
Uruguay
30°S
D
Argentina
Juan Fernández Ridge
30°S
Polonio High
SOUTH AMERICAN PLATE
Austral Segment
Malvinas-Falkland Current
Mid-Atlantic Ridge
Southern Andes
40°S
AFRICAN PLATE
Agulhas - Falkland Fracture Zone
40°S
SCOTIA PLATE
50°S
ANTARCTIC PLATE
Drake Passage
50°S
Antarctic Circumpolar Current
ANTARCTIC PLATE
60°S
80°W
60°W
40°W
20°W
600 km
60°S

Figure 1. Map of southern South America showing the main structures on land and in the southern Atlantic Ocean and the location of the Pelotas Basin with its northern and southern limits. Areas: SRS = Sul-Riograndense Shield; Rivers: A = Jacuí; B = Camaquã; C = Piratini; D = Rio de la Plata. Fracture zones and sub-basins according to Stica et al. (2014) and Serrat (2021). Ocean currents according to Stramma and England (1999), Laprida et al. (2011) and Santos et al. (2017).

The Pelotas Basin fill starts with subaerial basaltic lavas of the Imbituba Formation that overlie the basement of extended continental crust. These lavas are characterized in seismic images by packages of overlapping reflectors that are wedge-shaped and plunge towards the ocean (Bueno et al., 2007, Stica et al., 2014). They have no apparent basal termination and are locally convex upwards. Reflectors like these are common at extended margins, where they are called Seaward Dipping Reflectors (SDR). The Imbituba Formation SDRs form the first of two such packages in the basin, labelled as SDR1 (Fig. 2B) (Abreu, 1998; Bueno et al., 2007). Overlying SDR1, syn-rift sediments with alluvial and lacustrine facies associations represented by interlayered conglomerates, sandstones, and siltstones make up the Cassino Formation (Fig. 2B). Above this formation, a second SDR package (SDR2), related to submarine volcanic extrusions of the Curumim Formation, is recorded (Fig. 2B) (Abreu, 1998; Bueno et al., 2007) (Fig. 2B).

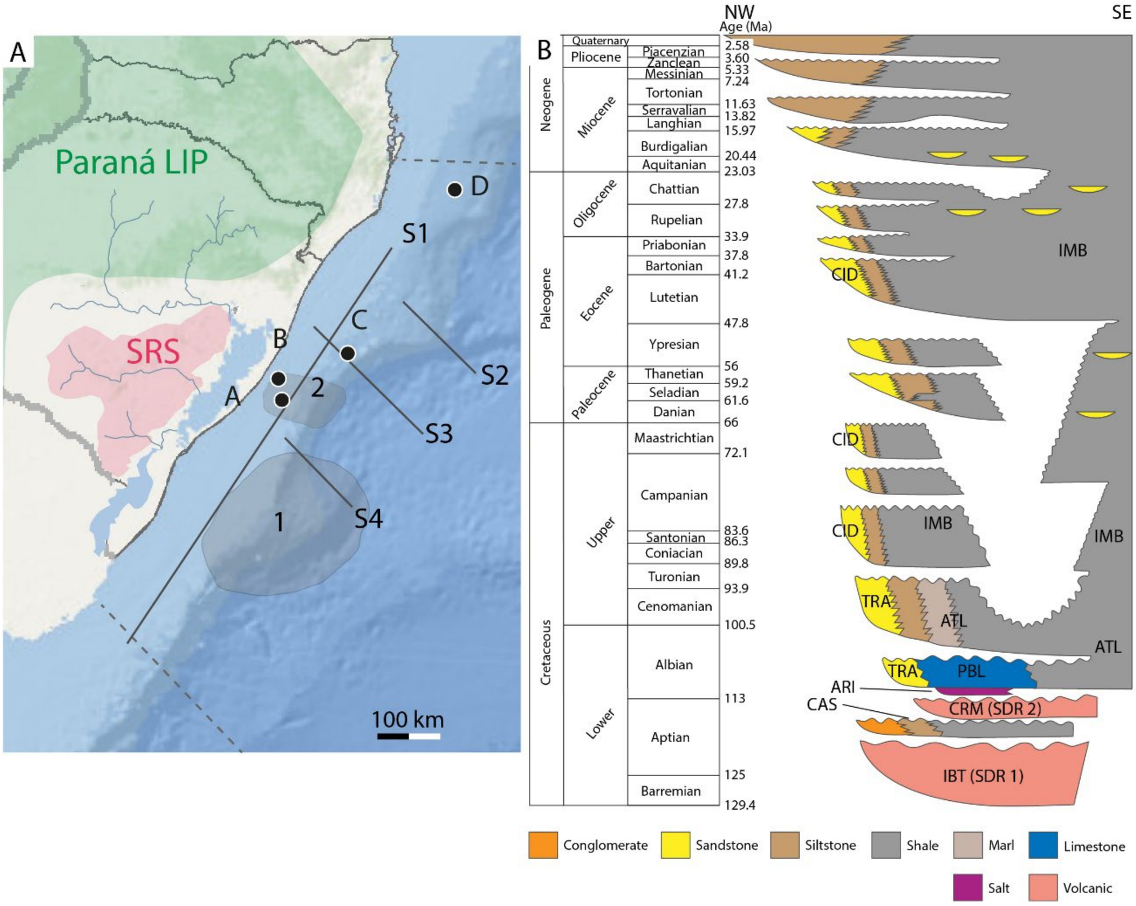

Figure 2. A) Map of the Pelotas Basin with interpreted seismic sections and wells. Seismic sections: S1 = 0034-0005, S2 = 0231-1349, S3 = 0228-0317, S4 = 0277J99B342. Wells: A = 1-RSS2-RS, B = 1-RSS3-RS, C = 2-RSS1-RS, D = 1-SCS2-SC. SRS = Sul-Riograndense Shield; 1 = Rio Grande Submarine Fan; 2 = Mostardas Low. B) Chronostratigraphic chart of the Pelotas Basin adapted from Bueno et al. (2007) and International Chronostratigraphic Chart 2020/1 from Cohen et al. (2013; updated). Formations: IBT = Imbituba, CAS = Cassino, CRM = Curumim, ARI = Ariri, PBL = Porto Belo, TRA = Tramandaí, ATL = Atlântida, CID = Cidreira, IMB = Imbé. Lower Cretaceous volcanic packages are also labelled as SDR packages SDR1 and SDR 2.

The drift phase began at the transition between the Aptian and Albian (Fontana, 1996) and continued until the present. The Cenozoic record of the Pelotas Basin consists of coastal environment deposits dominated by thick and thin clastic fans of the Cidreira Formation that give way laterally to distal deep marine shales and siltstone of the Imbé Formation, which also contains turbiditic deposits (Fig. 2B). From the Oligocene onwards, the clastic fans and deltas spread over the distal deposits, forming a large regressive sedimentary wedge in the Neogene (Bueno et al., 2007). The Rio Grande Submarine Fan (RGF) started to form in this context of increased sedimentary input (Abreu, 1998; Bueno et al., 2007, Rosa, 2007; Castillo-López, 2009) (Figs. 1 and 2A).

3. Material and Methods

We used Pelotas Basin public data; well logs and seismic sections available from the National Agency of Petroleum Gas and Biofuels (ANP). We applied three techniques: backstripping, seafloor spreading rate analysis, and seismic section interpretation. The spreading rate analysis was calculated for the entire sector of the Pelotas Basin. Figure 2A locates the four wells used in the backstripping calculation and the five seismic sections we interpreted.

The backstripping, seafloor spreading rate and seismic interpretation followed the workflow showed in the Figure 3. The following sub-items detail the methods.

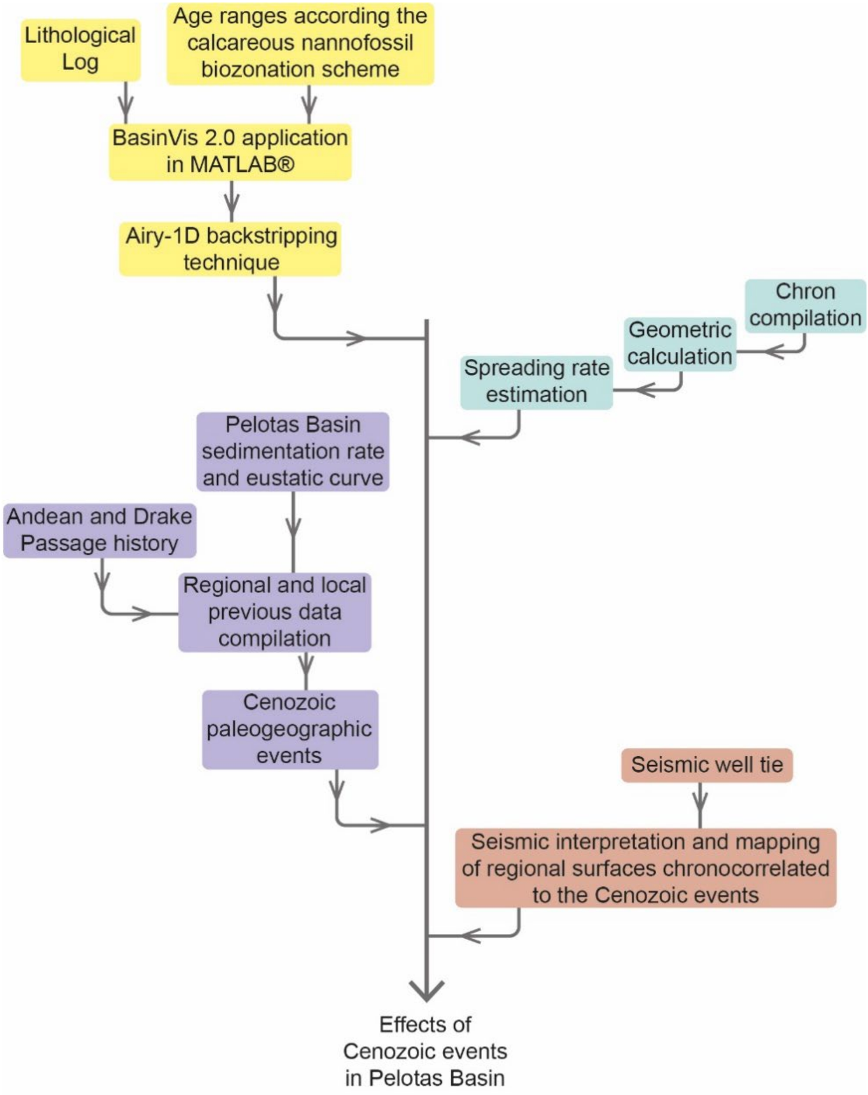

Figure 3. Methodological workflow applied in the identify the effects of Cenozoic events in Pelotas Basin.

3.1 Backstripping

The Airy-1D backstripping technique (Watts and Ryan, 1976) enables evaluation of the evolution of accommodation space. In this work, accommodation and total subsidence are considered synonyms. We performed the backstripping calculation using the BasinVis 2.0 application in MATLAB® (Lee and Wagreich, 2018) and data from 4 wells in the Pelotas Basin (Fig. 2A). By the stepwise removal of eustatic, sediment, and water loading signals for individual dated basin fill packages, the technique isolates a basin depth history that is interpretable in terms of tectonic controls uplift and subsidence (Lee et al., 2019).

The application of this technique starts from the analysis of total subsidence. This analysis involves restoring each sedimentary layer to its original thickness for a specific time and depth after using a compaction trend to remove the above sediment load. Assuming the total volume of sediment does not change with decompaction, the sediment column expands by increasing in porosity space. Equations for the reduction in porosity with increasing burial depth describe exponential trends (Sclater and Christie, 1980) (Equation 1):

$$\emptyset = \emptyset_0 exp^{-\mathrm{cz}} \qquad (1)$$

in which $\emptyset$, the porosity at depth, z, depends also on the uncompacted porosity at sea level, $\emptyset_0$ and a lithology-specific compaction coefficient, c. The total thickness of the restored sediment column defines the base for the total subsidence analyses. According to Gallagher and Lambeck (1989), the necessary parameters can be taken from a simplified lithological log (see Supplementary Material SM2 – Lithological log). The age ranges were parameterized according to the calcareous nannofossil biozonation scheme by Gomide (1989) and Antunes et al. (2004) (Supplementary Material SM1 – Biozonation). For practical purposes, the basement was considered any biozone corresponding to N340 or older (Supplementary Material SM1 – Biozonation).

From equation (1) (Sclater and Christie ,1980), we were able to compute the decompaction of a sediment column (Equation 2):

$$z2' - z1' = z2 - z1 - \frac{\emptyset_0}{c}\left(exp^{-cz1} - exp^{-cz2}\right) + \frac{\emptyset_0}{c}\left(exp^{-cz1'} - exp^{-cz2'}\right) \quad (2)$$

Where $z2$ and $z1$ are the actual depths of the sedimentary column (bottom and top), and $z2'$and $z1'$ are the decompacted depths of the sedimentary column (bottom and top) after removing overlying layers of sediment. Granted that $z1'$ is the paleobathymetry of the target time step, it is possible to solve $z2'$ numerically.

The tectonic subsidence consists of subsidence induced by tectonic processes (Steckler and Watts, 1978). It shows an ideal subsidence history by only considering the depth of a water-filled basin without the sediment-driven subsidence (Xie and Heller, 2009). The tectonic analysis comprises an isostatic balance between the lithospheric column through the sedimentary basin and a column in which the sedimentary load was removed and substituted by water. Further corrections are then applied for decompaction, paleobathymetry, and changes in eustasy. Paleobathymetry was based on the values presented by Koutsoukos (1982). For the eustatic curve, values from Abreu and Anderson (1998) were used. The 1D compensated tectonic model (Z) for any geological time t, is thus obtained with

$$Z(t) = S(t).\left(\frac{\rho_m+\rho_s}{\rho_m-\rho_w}\right) + W_d(t) - \Delta_{SL}(t).\left(\frac{\rho_m}{\rho_m-\rho_w}\right) \qquad (3),$$

where $S(t)$ refers to the decompacted sediment layer depth at any time (t), and ρ_m, ρ_s and ρ_w are the mean densities of the mantle (3300 kg/m^3), sediments (2300 kg/m^3), and water (1000 kg/m^3), respectively. $W_d(t)$ refers to the paleobathymetry at time t, and Δ_{SL} the change of eustatic sea-level between time t and the present (Lee et al., 2019).

3.2 South Atlantic spreading rate

Seafloor spreading rate variations can be estimated from the spacings of magnetic reversal isochrons on individual ship-track profiles (Pérez-Díaz et al., 2020). To calculate the spreading rate at the South Atlantic Mid-Ocean Ridge (SAMOR) at the latitude of the Pelotas Basin, we used the data set compiled by Seton et al. (2014) from the isochrons of Cande et al (1988), Müller et al (2008) and Pérez-Díaz and Eagles (2014). The studied interval pertains to the period of oceanic crustal accretion between chron C27n (60.92 Ma; Gee and Kent, 2007) and present. This interval excludes the effect of Rio Grande Rise-related ridge jumps (Pérez-Díaz and Eagles et al., 2017). Due to the minor change in the SAMOR position and geometry since 60 Ma (anchored to spin axis – Müller et al., 2016), we can reliably define the spreading rate based on the rate between time interval versus spacing of reversal isochrons on the west side of SAMOR.

To improve the reliability of our data, we measured along three different tracks between pairs of the main fracture zones: (I) the Tristan da Cunha and Chui fracture zones; (II) the Chui and Porto Alegre fracture zones; and (III) the Porto Alegre and Rio Grande fracture zones, that cross the Pelotas Basin sector. The spreading rate was then estimated from the mean values determined from isochron spacings between the three pairs of fracture zones.

3.3 Seismic Interpretation

Seismic interpretation was performed using Petrel 2020 software. The well-seismic tie was based on well biostratigraphic data. The biozonation used is Gomide (1989) and Antunes et al. (2004) (see Supplementary Material SM1 –

Biozonation). The regional surfaces were mapped and interpreted in time domain seismic sections.

4. RESULTS

4.1 Backstripping

The tectonic component curves (Fig. 4) behave similarly in four wells in the central and northern portions of the Pelotas Basin (Fig. 1 and 2A). The model subsidence curves show a notable inflection in the tectonic component at Upper Ypresian (50 Ma) times, whilst the total accommodation curves do not vary. Specifically, the sedimentary packages recorded in the wells reveal relatively continuous tectonic subsidence until 50 Ma, which in each case is followed by negative subsidence by amounts ranging between 200 m and 250 m, lasting until about 48 Ma (Fig. 4). Afterwards, there is a return to positive subsidence.

Both components of the model subsidence curves (tectonic and total) show little to no change across the Eocene-Oligocene boundary (ca. 34 Ma; Fig. 4). However, a few million years later, at Rupelian (30 Ma), all of the well sites start to experience a phase of relatively fast tectonic subsidence accompanied by enhanced total subsidence. In this interval, the tectonic subsidence ranges between 250 m and 300 m (Fig. 4). In this period, the deepest paleobathymetry is reached (Fig. 4).

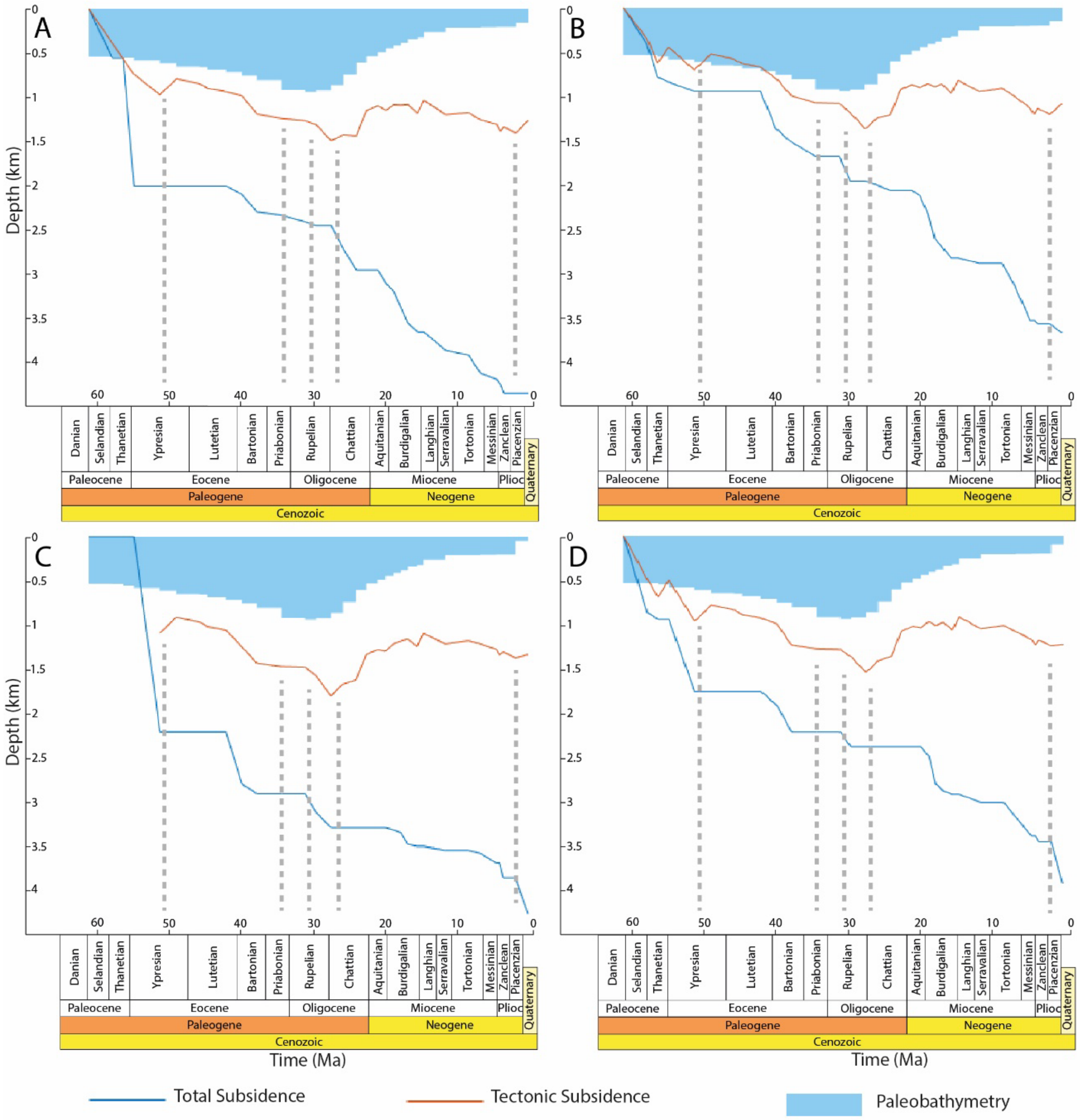

Figure 4. Backstripping results from four wells (A = 1-SCS-2-SC, B = 2-RSS-1-RS, C = 1-RSS-3-RS, D = 1-RSS-2-RS) in the Pelotas Basin (for locations, see Figure 2A). The grey dotted lines indicate ca. 50 Ma, 34 Ma, 30 Ma, and 27 Ma.

Chattian times (27 Ma) see an inflection in the tectonic component curve leading to renewed negative tectonic subsidence, which at the various well sites gradually tails off at different times during the 22-15 Ma period (Fig. 4). Afterwards, the sedimentary packages return to recording relatively slow tectonic subsidence followed finally by negative tectonic subsidence starting in the Piacenzian (2.5 Ma).

4.2 South Atlantic spreading rate

The South Atlantic spreading rate at latitudes that include the Pelotas Basin varies throughout the Cenozoic. In general, the plotted rates vary between approximately 1.5 cm/year and 3 cm/year (Fig. 5).

Spreading rates increase by 70% during the Ypresian (56 Ma to 47.8 Ma), from 1.4 cm/year to 2.4 cm/year (Fig. 5). Subsequently, they decrease slightly until Rupelian times (30 Ma), reaching 2.0 cm/year. Shortly afterwards, in Chattian times at 27 Ma, a short-lived spike sees the highest rate of plate divergence (2.9 cm/year) reached. After this interval, the divergence rate gradually decreases.

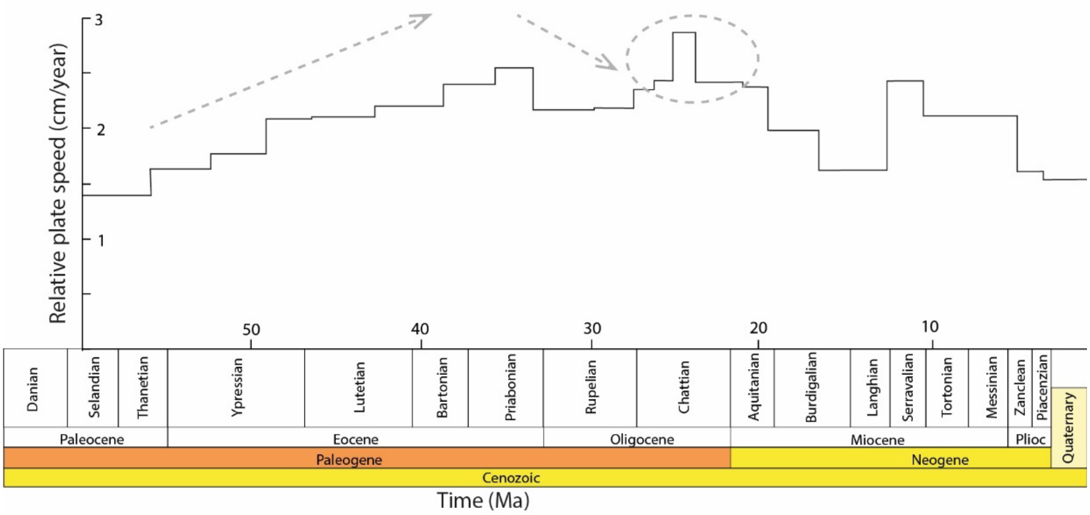

Figure 5. Spreading rates over the last 61 million years (a proxy for relative displacement of the South American plate) at the latitudes of the Pelotas Basin (compiled by Seton et al., 2014 from Cande et al., 1988; Müller et al., 1999 and Pérez-Díaz and Eagles, 2014 isochrons). The dotted arrows and circle highlight an initial acceleration, subsequent deceleration, and a short-lived spike to reach a maximum value.

4.3 Seismic Interpretation

The strike section of Fig. 6 shows a Chattian (27 Ma) reflector that divides two packages of contrasting reflector characteristics, resulting in different sismofacies described in this seismic section. In the package below it, reflectors are inclined towards the centre of the basin. This package is restricted to latitudes corresponding to the Mostardas Low (Figs. 1 and 2A). This sismofacies presents high amplitude reflectors, with lateral continuity and with stratified divergent internal reflection pattern. Above the Chattian reflector, widespread continuous reflectors dip very gently southwards, where the RGF is currently located (Figs. 1 and 2A). This package presents lateral continuity and stratified parallel to divergent internal reflection pattern. This interval can be divided in two sismofacies according with the amplitude: northeastward the reflectors present high amplitude, whilst southwestward the reflectors presents low amplitude.

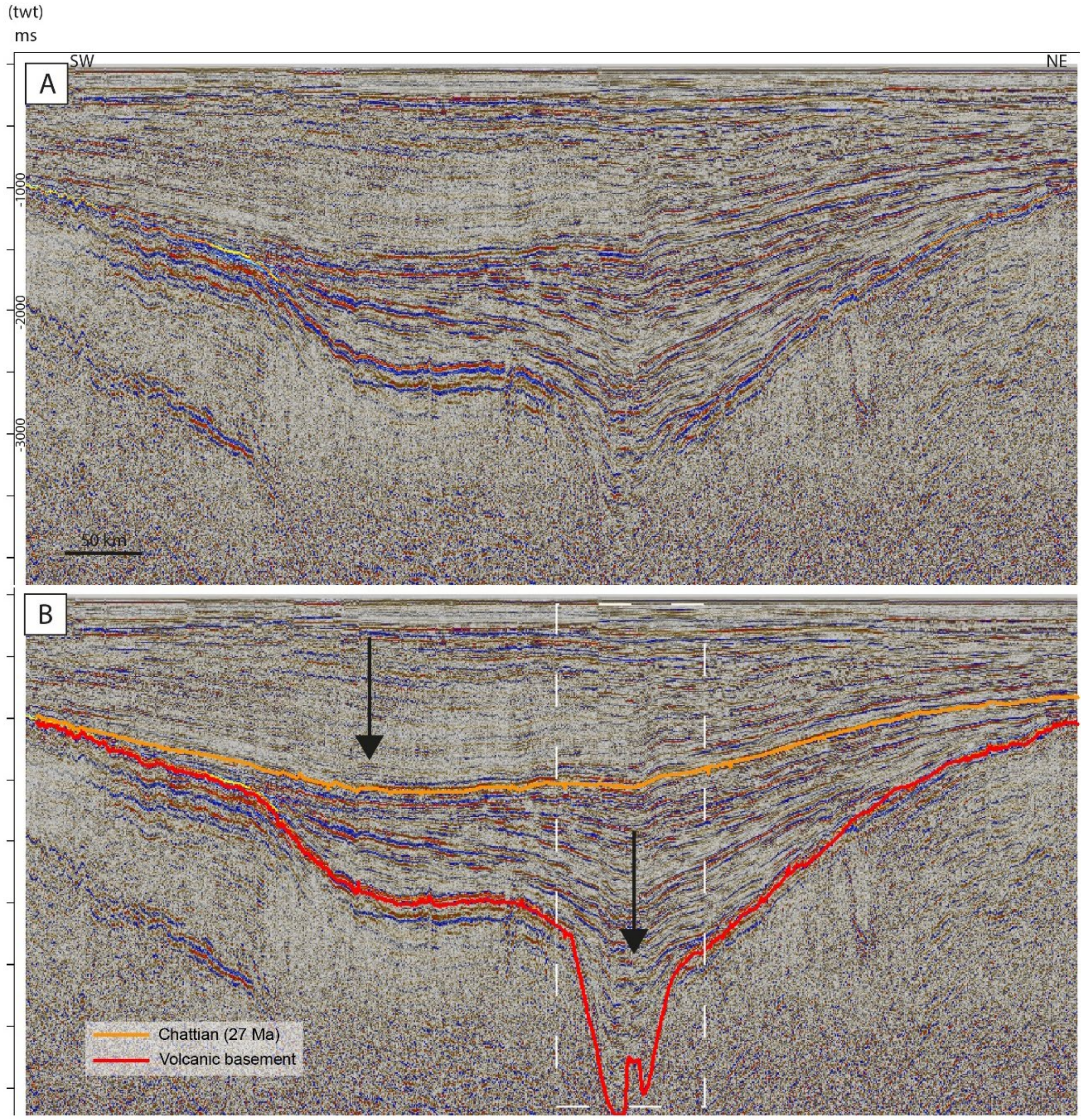

Figure 6. Pelotas Basin seismic sections on the continental platform (located as "S1" in Figure 2A). A) Strike section 0034-0005 without interpretation. B) Strike section 0034-0005 showing the volcanic basement and the Chattian (27 Ma) reflectors. The arrows indicate two depocenters and the dashed white rectangle indicates latitudes corresponding to the Mostardas Low.

The dip section over the RGF in Figure 7 also reveals a large-scale Oligocene-Miocene changes across the Chattian reflector (27 Ma) as observed in the strike section. The Chattian boundary coincides with the basal surface of a wedge-shaped macroform. This macroform displays internal reflectors with onlap and downlap terminations. Its upper limit is marked by the Aquitanian (20.60 Ma) reflector (Fig. 7).

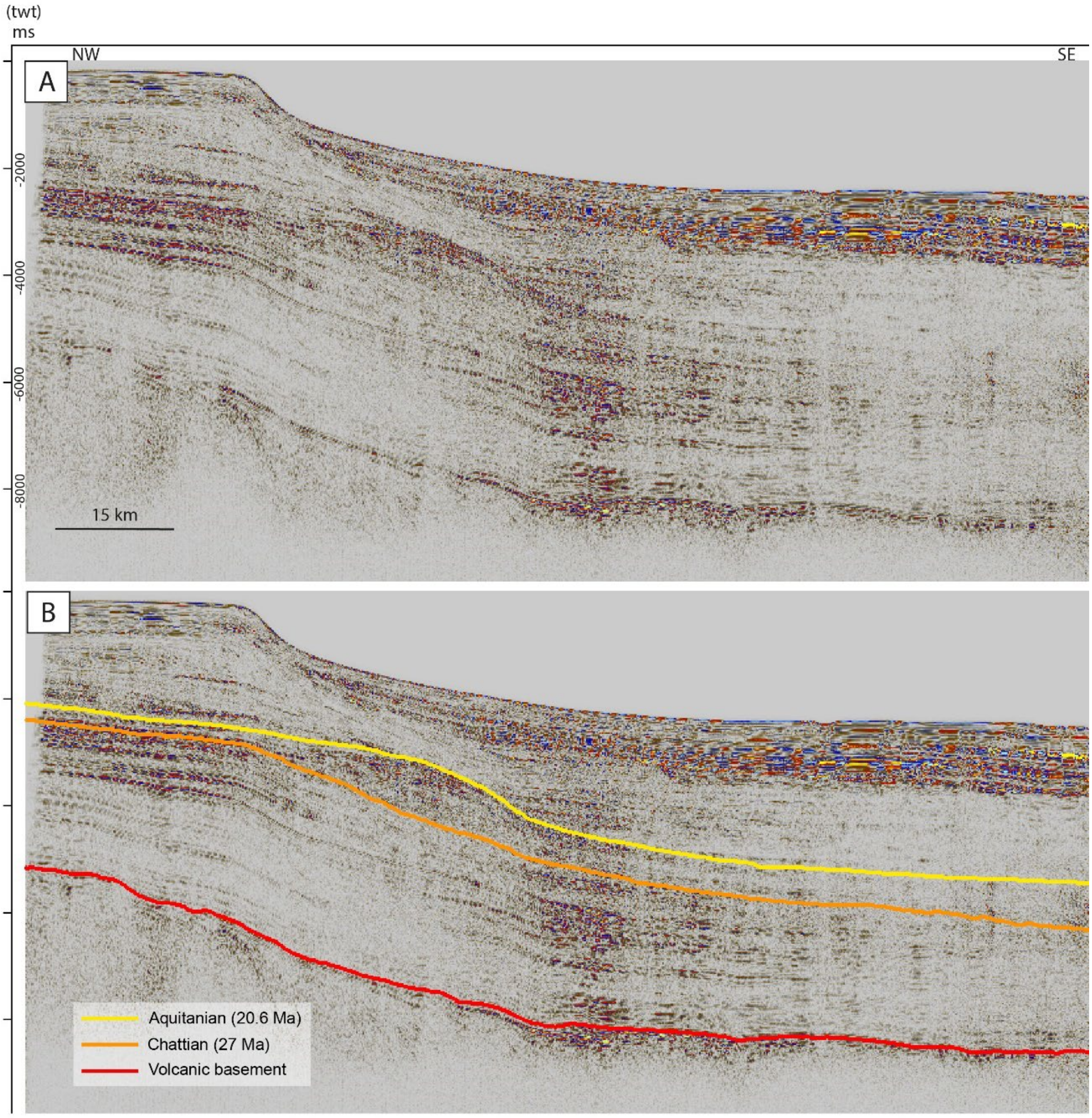

Figure 7. Southern Pelotas Basin seismic sections located as “S4” in Figure 2A. A) Dip section 0277J99B342 without interpretation. B) Dip section 0277J99B342 with interpretation of the volcanic basement, Chattian (27 Ma), and Aquitanian (20.60 Ma) reflectors. Note the wedge-shaped macroform between the orange and yellow reflectors.

The interpreted seismic dip sections (Figure 8) also allow mapping of relevant broadly continuous surfaces across the basin. One of these is an Ypresian (50 Ma) erosive surface, identifiable from prominent erosional truncation covered by onlap terminations. A second widespread erosive surface is interpretable in the Oligocene package, also identifiable by erosional truncation covered by onlap terminations. Above these, a Rupelian (30 Ma) flooding surface can be interpreted from widespread downlap terminations, what indicates a downlap surface, covering parallel to subparallel reflectors with onlap terminations (Fig. 8B).

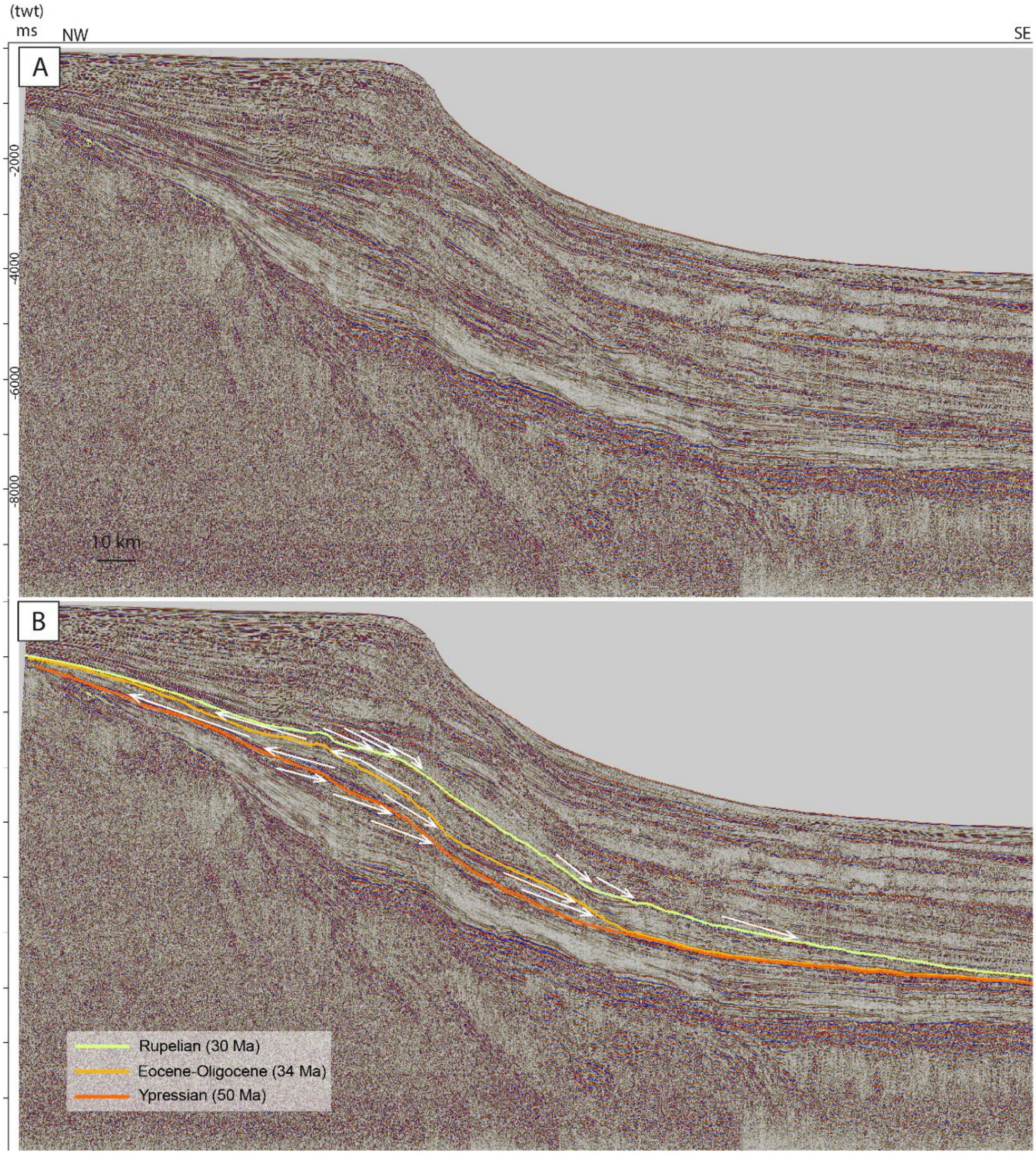

Figure 8. Central Pelotas Basin seismic section located as “S3” in Figure 2A. A) Dip section 0228-0317 without interpretation. B) Dip section 0228-0317 with reflector interpretation corresponding to erosive and flooding surfaces identifiable from stratal terminations (white arrows): Ypresian (50 Ma) erosive surface, Eocene-Oligocene (34 Ma) erosive surface, and Rupelian (30 Ma) flooding surface.

The seismic dip sections supported interpretations of depositional features. A thick package of reflectors is highlighted occurring above the Aquitanian reflector (20.60 Ma) (Fig. 9A). This package presents high amplitude reflectors, with varied lateral continuity and internal reflection pattern. This occurs because in the same interval the reflectors show stratified parallel to subparallel internal reflection pattern, which changes laterally to a divergent basal-concave internal reflection pattern that forms a channel geometry and channel fill. In the same level this channel geometry changes laterally to a convex external form with stratified aggradational internal reflection pattern, with a mounded geometry (Fig. 9B).

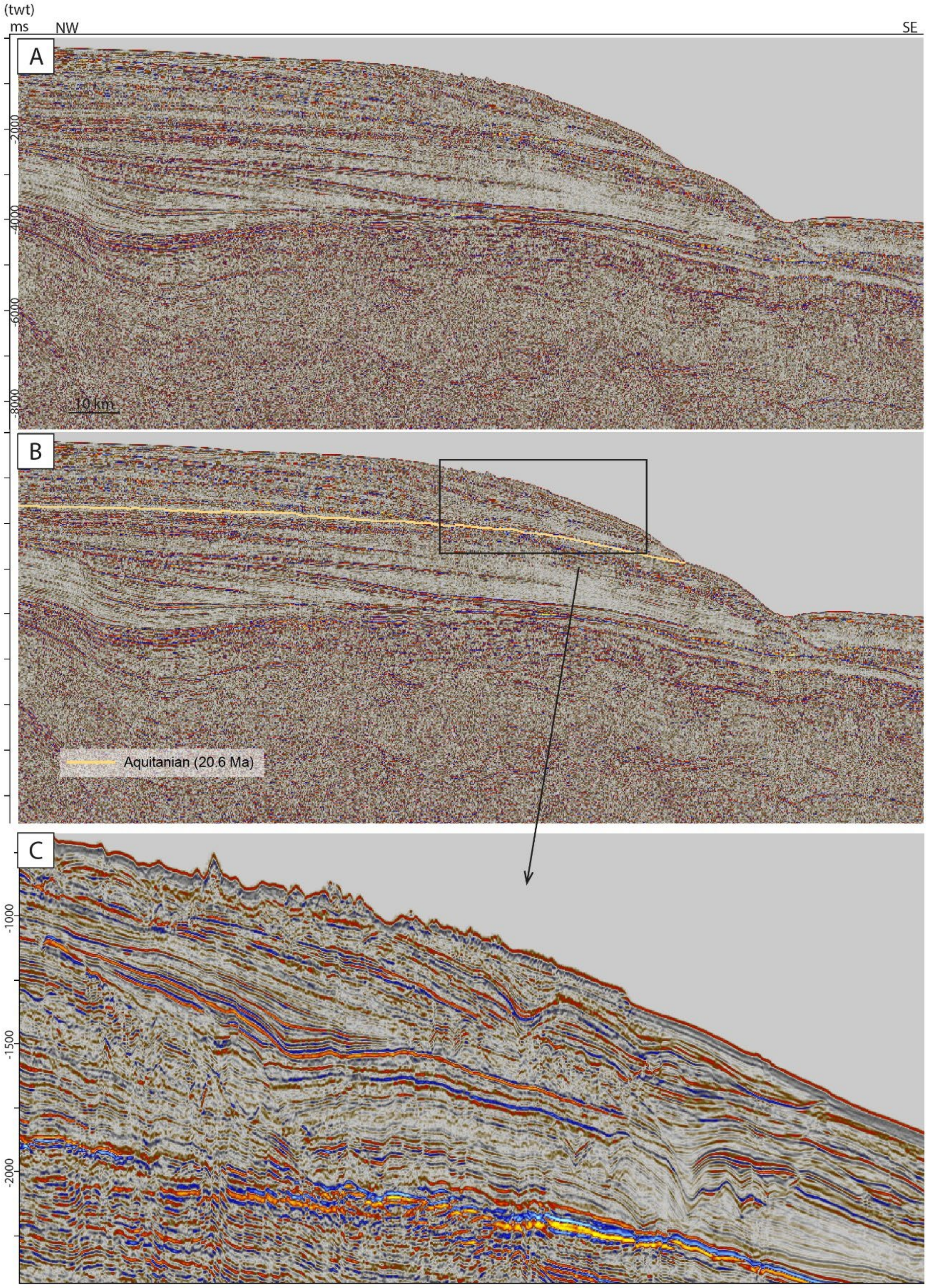

Figure 9. Northern Pelotas Basin seismic sections located as “S2” in Figure 2A. A) Dip section 0231-1349 without interpretation. B) Dip section 0231-1349 with Aquitanian (20.60 Ma) reflector. C) Detailed section showing the interval where the reflectors change the parallel-subparallel patterns to a localized channel-type geometries.

5. DISCUSSION

The results indicate that the Cenozoic filling history of the Pelotas Basin shows temporal correlations with large scale paleogeographic and paleoclimatic events. Integrating the results of the present work with available data of the regional geology and Cenozoic history, we can construct a model of tectonic, glacioeustatic and climatic controls on sedimentation in the basin.

5.1 Eocene (50 Ma), Oligo-Miocene (27 Ma) and Pliocene (2.5 Ma) Uplifts

The backstripping results from all analysed wells show a decrease in tectonic subsidence at 50 Ma (Ypresian; Figs. 4 and 10F). This ubiquitous signal indicates basinwide uplift. Associated with the uplift, a hiatus is evident from flat sections in the total accommodation curves (Figs. 4 and 10G). The seismic interpretation shows an accompanying widespread erosional surface (Fig. 8B). The uplift, hiatus, and erosion all occur during a period of increasing South Atlantic seafloor spreading rates (Figs. 5 and 10D). A comparable set of associations is seen in Chattian times (27 Ma). The tectonic subsidence component decreases in all of analysed wells and is accompanied by hiatuses. The basinal depocenter shifts from the basin’s central sector to its southern sector, as revealed by a significant change between the Oligocene and Miocene described in the seismic interpretation. The South Atlantic's spreading rate reaches its highest speed of 2.9 cm/year. After Chattian (27 Ma), the following change in the model subsidence curve is a decrease that occurred only at Piacenzian in the Pliocene (2.5 Ma).

Koutsoukos (1982), Gomide (1989), and Anjos-Zerfass et al. (2014) all identified Ypresian hiatuses in wells along the Rio Grande do Sul coast (Fig. 10B). An age progression amongst these hiatuses suggests that deposition stopped earlier in the south than in the north within the basin (Anjos-Zerfass et al., 2008). At the same time, the data of Abreu and Anderson (1998) show an isolated eustatic fall superimposed on a period of relatively higher values (Fig. 11D). The highest Cenozoic global average temperatures are reached in this interval, culminating in the Early Eocene Climatic Optimum, correlating with the later uplift events we have characterized (Fig. 10E). A comparable occurrence of data is reported in Oligo-Miocene times. Anjos-Zerfass et al. (2014) where identified further hiatuses from Upper Oligocene (Chattian) and Lower Miocene (Aquitanian and Burdigalian) well data (Fig. 10B). The data from Abreu and Anderson (1998) show a considerable eustatic fall in this interval (Fig. 10C).

Along the Cenozoic, the southern South America paleogeography changed. During the Ypresian, the southern tip of South America remained connected to the Antarctic Peninsula by a land bridge where the Drake Passage and the Scotia Sea are located today (Fig. 11A and 11F). However, at approximately 50 Ma, the increase in the separation rate between the South American and Antarctic plates caused rotational and compressional movements in southern South America, resulting in deformation in the Tierra del Fuego region (Livermore et al., 2007). A comparable occurrence is reported in Oligo-Miocene times, when the increase in the separation rate between South American and Antarctic allowed a full-depth route between Pacific and Atlantic oceans (Fig 11D e 11E).

Northward, the Southern and Central Andes are marked by significant compressional, neutral, and extensional regimes changes during the Cenozoic. Such changes are related to heterogeneities in the speed and angle of subduction along the convergent plate boundary (Carrapa et al., 2014, Horton, 2018). The Southern Andean sector was configured by the predominance of an extensional regime possibly related to slab rollback in a retreating subduction system (Horton, 2018). On the other hand, with a lower angle and subduction rate, the Central Andean sector was dominated by a compressional regime. In the same way that between southern South America and Antarctica, the Central Andes also showed pulsed changes (Horton, 2018, Quade et al., 2014). Cenozoic record three main uplift pulses in the Central Andes, mainly in the NW region of Argentina: a) the Domeyko Cordillera and the Puna Plateau at 50-40 Ma, b) the East Cordillera at 25-15 Ma, and more recently, c) the Sub-Andes starting at 5 Ma. These three pulses are directly related to the increases in the subduction speed rate of the Nazca Plate under South American Plate (Fig. 10G) (Pardo-Casas and Molnar, 1987, Quade et al., 2014).

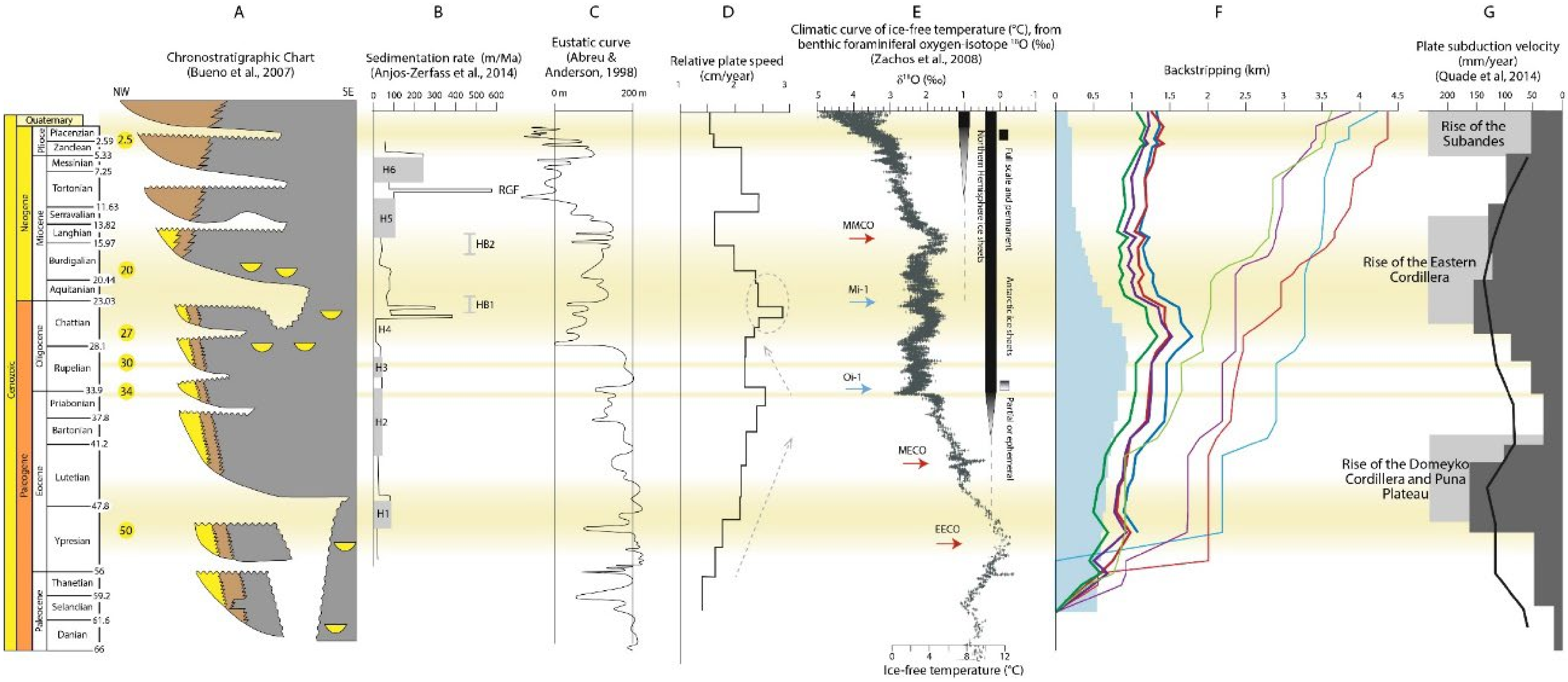

Figure 10. Compilation of Cenozoic geological events. A) Pelotas basin chronostratigraphic chart from Bueno et al. (2014). Yellow circles mark events identified in the Pelotas Basin in this work. B) Sedimentation rates from Anjos-Zerfass et al. (2014). Grey areas represent the hiatuses identified in two different wells. C) Eustatic curve from Abreu and Anderson (1998). D) Speed of the South American plate relative to the African plate in latitudes corresponding to the Pelotas Basin (based on isochrons compiled by Seton et al. (2014). E) Climatic curves from Zachos et all (2008) stacked benthic foraminiferal oxygen isotope curves. Oceanic δ18O changes directly due to temperature fluctuations; high values represent cold climates, while lower values indicate a warm climate. MMCO = Middle Miocene Climatic Optimum, Mi-1 =, Oi-1 =, MECO = Mid-Eocene Climatic Optimum, EECO = Early Eocene Climatic Optimum. F) Curves resulting from the backstripping. The thicker curves represent the tectonic component, and the thinner curves represent the total accommodation. Wells indicated by colour: green = 2-RSS-1-RS, purple = 1-RSS-2-RS, red = 1-SCS-2-SC, blue = 1-RSS-3-RS. The light blue area represents paleobathymetry. G) Values of the Nazca Plate subduction speed (Pardo-Casas and Molnar, 1987) and their correlation with uplift events in the Central Andes (Quade et al., 2014).

From Figures 10 and 11, it is possible to observe correlations between a) Pelotas Basin tectono-sedimentary events reported in this work (uplifts observed in the backstripping, the erosive surface described in seismic interpretation, fluctuations to the increase in relative South American plate speed), b) Pelotas Basin previous literature (hiatuses and eustatic falls reported by Anjos-Zerfass et al. (2014) and Abreu and Anderson (1998)) and c) Cenozoic history regional-scale data of Andes and southern South Atlantic.

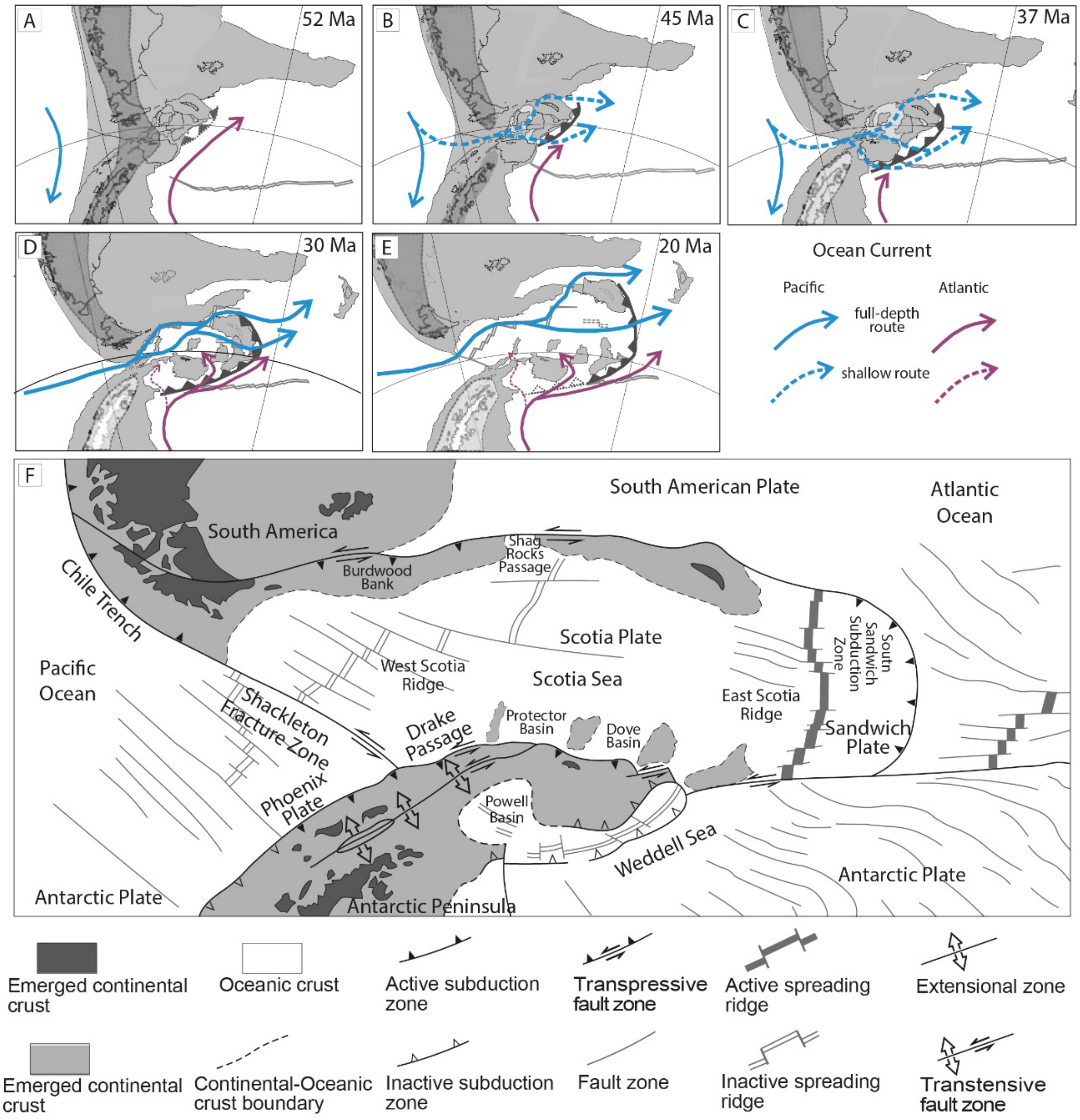

Figure 11. Development (A, B, C, D and E; adapted from Livermore et al., 2007 and Livermore et al., 2005) and current state (F, adapted from Galindo-Zaldívar et al., 2014) of the Drake Passage and Scotia Sea.

Theses correlations enable to infer cause-and-effect relationships between the sedimentary record of subsidence and uplift in the Pelotas Basin and the tectonics of the Central Andes, precisely the Eocene, Oligo-Miocene, and Pliocene uplifts. Tectonic Andean uplift in the South American plate western margin may have had a long wavelength component that affected the Pelotas Basin further east. Thus, the cause of the uplift events and tilting in the Pelotas is associated with the transmission of subduction-related compressional stresses.

Additionally, since the Andean Central uplifts (Fig. 10G) and the divergence rate increases between South America and Antarctica (Fig. 11) occurs under similar Eocene and Oligo-Miocene time spans (Fig 10), both whilst South Atlantic spreading rate is high or, at least accelerating, it is possible to infer the interaction between South American, Nazca and Antarctic plates in response to SAMOR spreading rate. The clear link appears to be an increase in the rate of motion of the South American plate over the mantle. Considering the speed and angle heterogeneities in the subduction along the South American plate convergent boundary (Carrapa et al., 2014, Horton, 2018) it is expected that each tectonic domain results different responses. In this case a) uplift pulses responding to compressional domain in Central Andes and b) divergence increase pulses between South America and Antarctic responding to extensional domain in southern tip of South America and Southern Andes.

5.2 Oligocene Glaciation (34 Ma)

The model subsidence curves show lower Oligocene stability in both the tectonic and total components (Figs. 4 and 10F). This stability indicates a low generation of accommodation space, leading to sedimentation hiatuses (Fig 10B) and the formation of a broad and continuous erosional surface in the basin (Fig. 8). These events accompanied a eustatic sea level drop, according to the study of Abreu and Anderson (1998) (Fig. 10C), and the early Oligocene glaciation event (Oi-1) recorded the δ18O ratio proxy for global temperature and ice volume, and other proxies for atmospheric CO_2 concentration (Zachos et al., 2008, Wright, 2009, Mudelsee et al., 2014) (Fig. 10E). Oi-1 occurred just 3 Myr after Livermore et all (2007) estimate for the time at which deep water mixing between the South Atlantic and Pacific Oceans would have been possible across the widening Drake Passage (Fig. 11C).

The most plausible explanation for the temporal correlation between the Oi-1 events and low accommodation space generation and hiatus development in the early Oligocene of the Pelotas Basin is eustatic sea level fall related to the rapid growth of the Antarctic ice sheet. In other words, in the Pelotas Basin, the beginning of Antarctic glaciation is expressed by an erosive horizon visible in the seismic sections, caused by a eustatic fall resulting from the advance of a polar ice mass.

5.3 Flooding during the Oligocene (30 Ma)

In the middle Oligocene, at approximately 30 Ma, both sets of curves resulting from the backstripping analysis display an increase in subsidence rate (Figs. 4 and 10F). Additionally, this time sees the deepest paleobathymetry develop (Figs. 4 and 10F), whilst South American plate speed decelerates and stabilizes (Figs. 5 and 10D), and the seismic sections reveal development of a widespread flooding surface (Fig. 8). At the same time, Abreu and Anderson (1998) eustatic curve shows the end of an expressive and extensive period of high global sea level (Fig. 10C). Vigorous deepwater flow (1000 m to 3000 m) would have first become possible through Drake Passage to occur permanently between the South Atlantic and the Pacific Oceans at around 30 Ma with the development of an organized mid-ocean ridge in the west Scotia Sea, the West Scotia Ridge (Fig. 11D and 11F) (Livermore et al., 2007). As consequence of the South American plate speed decelerates, this time span occurs between the highest rates of Nazca Plate subduction and consequent Central Andes Uplifts.

A plausible explanation for the temporal correlations between the results of increase in the subsidence, deepest paleobathymetry, South American plate speed decelerating, and a flooding surface is associated with Andean Uplifts and its triggering factors. The Pelotas basin may be affected by the intumescence of the oceanic crust when the South American Plate accelerate. Additionally, when the uplifts activity decreases, the sediment supply tends to proportionally decreases. These two factors contribute to the occurrence of transgression in the Pelotas Basin observed in the seismic as a flooding surface.

5.4 Antarctic Circumpolar Current (ACC) (20 Ma)

In the Miocene sequence of the Pelotas Basin we identified elongated mounded drifts that accumulated during sedimentation affected by contour currents (e.g. Rebesco et al., 2014). These thick contourite packages are recognized in strata dating from the Aquitanian (Fig. 9) to present. Identifying the drifts as contourites is possible due to the occurrence of channel-shaped and mounded reflection patterns visible in dip seismic sections, which means that elongated shapes occur parallel to the platform.

A significant reorganization of spreading centres in the Scotia Sea occurred at around 17-20 Ma (Livermore et al., 2007; Eagles and Jokat, 2014). Spreading rates in the West Scotia Ridge declined sharply as a new ridge started to operate in the East Scotia Sea (Fig. 11E). The widening of a deep passage between Burdwood Bank and Shag Rocks at that time established a pattern of more intense ACC flow similar to today's (Fig. 1) (Livermore et al., 2007).

The intensified ACC and permanently glacial Antarctica promoted steeper thermal and salinity gradients between the pole and the equator, leading to more vigorous thermohaline circulation. As part of this, the ACC interacts directly with the Malvinas and Brazil Currents in the Pelotas Basin (Fig. 1). Thus, the contourites of the Pelotas Basin resulted from the sum of the events that established the modern-style ACC.

5.5 Rio Grande Submarine Fan (RGF)

The RGF is a well-known geoform in the Pelotas Basin (Zalan, 2005; Rosa, 2007; Miller et al, 2015; Chemale et al., 2020). It is visible in satellite images as a protruberance in the continental shelf break in the southern portion of the basin (Fig. 1). Despite being called a cone and characterized as a deepwater submarine fan (Rosa, 2007), it does not show radial geometry. Away from the shelf break, its long axis is aligned SW-NE. The RGF reaches down to depths of 4000 m on the continental rise (Kowsmann and Costa, 1974; Rosa, 2007; Castillo-López, 2009). Its maximum width is 400 km, it has an area of 28,900 km² and a volume of 5.02943×10^{12} m³, owing to the very thick sedimentary succession of more than 5000 m (Rosa, 2007; Castillo-López, 2009). The RGF is composed of sedimentary wedges that thicken towards the shelf break, giving rise to large progradational sequences (Castillo-López, 2009). RGF sedimentation is predominantly pelagic, giving rise to a fan composed of shale, clay, silt and sparse intercalations of sandy lobes (Alves, 1977; Rosa, 2007). The Rio de la Plata (Fig. 1) delivers most of the fan’s sediments, some of which are siliciclastic sediments of Andean origin, but there are smaller contributions of diverse Phanerozoic and Neoproterozoic clasts from sources around the Paraná Basin and crystalline basement of Sul-Riograndense Shield (Fig. 1; Martins et al., 1972; Urien et al., 1978; Zouain, 1986; Castillo-López, 2009, Chemale Jr. et al., 2021, Rizzi et al., 2022). According to Fontana (1996), Zalan (2005) and Rosa (2007), one of the main structural elements is a major listric detachment linking an upslope population of extensional faults to a population of compressive faults at the slope toe, all of which can be related to wholesale gravity sliding of the fan sequence down the detachment. This structural complexity is interpreted as resulting from a detachment surface

Changing reflector characteristics between the basin's Oligocene and Miocene sections reveal a depocentre shift (Fig. 6) as described in the seismic interpretation. The onset of this change occurs approximately around the Chattian reflector (27 Ma) (Fig. 6). A wedge-shaped macroform developed into Miocene times (Fig. 7), whilst the depocentre moved away from the Mostardas Low towards the southern reaches of the basin where the RGF is located today. The 27 Ma reflector thus marks the onset of RGF sedimentation. A reduction in reflector amplitudes (Fig. 6) above the Oligocene-Miocene transition of the RGF marks a change to deposition of thick units of fine-grained sediments. These events started at the same time as an uplift pulse in the Eastern Andean Cordillera (Fig. 10G) (Quade et al., 2014). The Eastern Cordillera is a close segment of the Andes to the Pelotas Basin (Fig. 1), so that we suggest a link between the uplift and the depocentre shift, via compressional reactivation of old basement structures in the basin. The onset of deposition at the RGF may therefore ultimately have had a tectonic cause.

Submarine fans are known to have a very high sedimentation rate. Anjos-Zerfass et al. (2014) estimated rates of up to 600 m/Myr for the RGF. This is much higher than is typical for passive margins, where average rates of 20-100 m/Myr for siliciclastic shelves or 50-500 m/Myr for lower fans are to be expected (Einsele, 1992). Enhanced sediment supply to the RGF in the Pelotas Basin is consistent with the idea of a tectonic trigger from Miocene Andean uplift. In addition, rapid RGF sedimentation can be expected to have enhanced subsidence rates in the Pelotas Basin.

The increasing rate of Miocene sediment transport after the onset phase of the RGF is frequently attributed to Sul-Riograndense Shield by paleodrainages and Rio de la Plata (Martins et al., 1972; Urien et al., 1978; Zouain, 1986; Castillo-López, 2009). However, the processes and mechanisms controlling this increase remain to be detailed. One possible factor, as discussed above, might have been the broadening of the ACC and increased vigour of thermoholine circulation related to widening of Drake Passage since 20 Ma (Fig. 11). That these events affected the Pelotas Basin is well demonstrated by the onset of contourite sedimentation in response to slope-parallel transport via the cold Malvinas and warm Brazil currents (Fig. 1). These currents meet and mix in the Pelotas Basin (Chemale et al., 2021), where their contrasting temperatures have been postulated to enhance clay deposition by flocculation (Addai-Mensah, 2007).

This study thus establishes that the RGF is a compound megaform built in two distinct phases. Phase 1 corresponds to the package between the Chattian (27 Ma) and Aquitanian (20 Ma) reflectors. The Chattian (27 Ma) reflector stands out as the base of a progradational package identified by its wedge geometry and onlap (top) and downlap (base) reflector terminations. The wedge represents transport and deposition of sediments outwards into the basin, perpendicular to the platform break, related to the supply of sediments from the continental interior via its margin. Phase 2 corresponds to the thick package of reflectors above the Aquitanian (20 Ma) reflector. This package records longitudinal transport by currents running parallel to the shelf break. From 20 Ma onwards, with the onset of the ACC, the interaction between cold and warm currents may have played an important role in the deposition of sediments in the RGF area.

6. CONCLUSIONS

This work was performed based on the generation of backstripping results, South Atlantic spreading rate analysis, seismic interpretation in the Pelotas Basin, and published studies of the basin's sedimentation rate, paleobathymetry and biozonation. The results were interpreted in the context of published information about South American regional geological events, global and regional climatic, oceanographic, tectonic, and glacioeustatic influences on sedimentation in the basin.

Central and Southern Andean tectonics exerted recurrent influences on the Pelotas Basin. Eocene, Oligo-Miocene and Pliocene pulses of Andean deformation all correlate with tectonic uplift episodes revealed by our backstripping analysis, which corresponded to compressive events in the Central Andes. On the other hand, the opening of passages and straits resulted from divergence increase pulses between South America and Antarctic corresponded to extensional domain in southern tip of South America. Since these phenomena occurred whilst South Atlantic spreading rate is high or, at least accelerating, it is possible to infer the interaction between South American, Nazca and Antarctic plates in response to SAMOR spreading rate.

The importance of the gradual widening of the Drake Passage and consequent ACC is also evident in the sedimentation and subsidence history of the Pelotas Basin. These processes were responsible for generating glacioeustatic interference in the Oligocene section of the basin. Additionally, the widening of Drake Passage also conditioned the South Atlantic oceanographic setting so that contour currents, the Malvinas and Brazil currents, were influenced and played fundamental roles in sediment transport and deposition in the Pelotas Basin.

The genesis of the RGF is interesting because it can be related to both Andean and gateway-oceanographic forcings: 1) at 27-20 Ma, basinward transport and sedimentation sourced from the Sul-Riograndense Shield and Phanerozoic Paraná Basin, improved by the Andean-influenced uplift and consequent depocenter change and 2) from 20 Ma to present, in response to a long-slope sediment transport by contour currents and sedimentation facilitated by their mixing.

It is essential to highlight the tectonic compressive influence in the passive margin basins sedimentation. Finally, the cause-and-effect correlation between climate and tectonics becomes more robust with integrating methods and a systematic quantitative application and statistical treatment of data.

Acknowledgments

This project has been supported by UNISINOS-PETROBRAS Cooperation Agreement (#5900.0109881.18.9). The authors thank the Brazilian Agency of Petroleum, Natural Gas and Biofuels (ANP) for the data availability. Marlise Colling Cassel is grateful to Coordination for the Improvement of Higher Education Personnel (CAPES) for the Ph.D. scholarship. We thank Rodrigo Guerra for his contribution to the biozone studies and Geise Anjos-Zerfass for providing her chronostratigraphic data, and José Manuel M.T. de Oliveira and

Giuseppe de Toni for the enriching discussions. We thank the Editor Liviu Matenco, the revierwe Graeme Eagles and anonymous reviewer for constructive comments.

REFERENCES

Abreu, V.S.,1998. Geologic Evolution of conjugate volcanic passive margins: Pelotas Basin (Brazil) and offshore Namibia (Africa) Implication for global sea-level changes. Rice University, Houston.

Abreu, V.S., Anderson, J.B., 1998. Glacial eustasy during the Cenozoic: sequence stratigraphic implications. AAPG Bulletin 82, n. 7, 1385-1400.

Addai-Mensah, J., 2007. Enhanced flocculation and dewatering of clay minerals dispersions. Powder Technology 179, 73-78.

Alves, E.C., 1977. Estrutura rasa do talude e sopé da Margem Continental do Rio Grande do Sul e Uruguai. Universidade Federal do Rio Grande do Sul, Porto Alegre.

Anjos-Zerfass, G.S., Souza, P.A., Chemale Jr., F., 2008. Biocronoestratigrafia da Bacia de Pelotas: estado atual e aplicação na geologia do petróleo. Revista Brasileira de Geociências 38, 47-62.

Anjos-Zerfass, G.S., 2009. Estudos paleoambientais com base em isótopos de carbono, oxigênio e estrôncio em foraminíferos do Terciário da Bacia de Pelotas. Universidade Federal do Rio Grande do Sul, Porto Alegre.

Anjos-Zerfass, G.S., Chemale Jr., F., Moura, C.A.V., Costa, K.B, Kawashita, K., 2014. Strontium isotoppe stratigraphy of the Pelotas Basin. Brazilian Journal of Geology 44, n. 1, 23-38.

Antunes, R.L., Oliveira, L.C.V., Shimabukuro, S., Cunha, A.S., 1998. Calcareous nannofossil biozones of the brazilian continental margin: evolution of a concept. International Nannoplankton Association Conference 7, Puerto Rico.

Antunes, R.L.; Oliveira, L.C.V.; Rosa, A.Z.; Costa, S.O.; Cunha, A.S.; Lima, F.H.O. 2004. Em busca da bioestratigrafia de alta resolução – A performance do zoneamento de nanofósseis calcários da Petrobras. Boletim de Geociências da Petrobras, Rio de Janeiro, 12, n. 2, 421-427.

Bueno. G.V., Zacharias, A.A., Oreiro, S.G., Cupertino, J.A., Falkenhein, F.U.H., Neto, M.A., 2007. Bacia de Pelotas. Boletim de Geociências da Petrobrás 15, n. 2, 557-559.

Canavan, R. R., Carrapa, B., Clementz, M. T., Quade, J., DeCelles, P. G., & Schoenbohm, L. M. (2014). Early Cenozoic uplift of the Puna plateau, central Andes, based on stable isotope paleoaltimetry of hydrated volcanic glass. Geology, 42, 447–450.

Cande, S.C., LaBrecque, J.L., Haxby, W.F. 1988. Plate Kinematics of the South Atlantic: Chron C34 to present. Journal of Geophysical Research 93, 13479-13492.

Carrapa, B., Huntington, K.W., Clementz, M., Quade, J., Bywater-Reyes, S., Schoenbohm, L.M., Canavan, R.R., 2014. Uplift of the Central Andes of NW Argentina associated with upper crustal shortening, revealed by multiproxys isotopic analyses. Tectonics 33. doi:10.1002/2013TC003461.

Castillo-López, L.A., 2009. Interpretação sismoestratigráfica e geomorfologia sísmica do Cone de Rio Grande, Bacia de Pelotas. Universidade Federal do Rio Grande do Sul, Porto Alegre.

Chemale Junior, F., Lavina, E.L.C., Carassai, J.J., Girelli, T.J., Lana, C., 2021. Andean orogenic signature in the Quaternary sandy barriers of Southernmost Brazilian Passive margin – Paradigm as a source area. Geoscience Frontiers 12(4),101119. https://doi.org/10.1016/j.gsf.2020.11.015

Cohen, K.M., Finney, S.C., Gibbard, P.L., Fa, J.X. 2013 updated. The ICS International Chronostratigraphic Cjart. Episodes 36, 199-204.

Curray, J.R., Emmel, F.J., and Moore, D.G., 2003. The Bengal Fan: morphology, geometry, stratigraphy, history and processes. Marine and Petroleum Geology, 19(10), 1191–1223. https://doi.org/10.1016/S0264-8172(03)00035-7

Damuth, J., Kumar, N., 1975. Amazon cone: morphology, sediments, age, and growth pattern. GSA Bull. 6:863–878. http://dx.doi.org/10.1130/0016-7606(1975)86b863: ACMSAAN2.0.CO;2.

Eagle, G. and Jokat, W., 2014. Tectonic reconstructions for paleobathymetry in Drake Passage. Tectonophysics 611, 28-50.

Einsele, G., 1992. Sedimentary Basins Evolution, Facies, and Sediment Budget. Springer-Verlag, Berlin.

Fontana, R.L., 1996. Geotectônica e sismoestratigrafia da Bacia de Pelotas e Plataforma de Florianópolis. Doctorate thesis, Universidade Federal do Rio Grande do Sul, Porto Alegre, 216 p..

Galindo-Zaldívar, J., Puga, E., Bohoyo, F., González, F.J., Maldonado, A., Martos, Y., Perez, L.F., Ruano, P., Schreider, A., Somoza, L., Surinach, E., Antonio, D.F., 2014. Magmatism, structure and age of Dove Basin (Antarctica): A key to understanding South Scotia Arc development. Global and Planetary Change 122, 50-69.

Gallagher, K., Lambeck, K., 1989. Subsidence, sedimentation and sea-level changes in the Eromanga Basin, Australia. Basin Research 2, 115–131.

Gomide, J., 1989. Bacia de Pelotas: biocronoestratigrafia baseada e nanofósseis calcarios. Congresso Brasileiro de Paleontologia 11, 338-351.

Gee, J. S and Kent, D. V., 2007. Source of oceanic magnetic anomalies and the geomagnetic polarity time scale. Treatise on Geophysics, vol. 5: Geomagnetism, Elsevier, Amsterdam, pp. 455-507. https://doi.org/10.1016/B978-044452748-6.00097-3

Hoorn, C., Bogotá-A, G.R., Romero-Baez, M., Lammertsma, E.I., Flantua, S. G.A., Dantas, E.L., Din, R., do Carmo, D.A., Chemale Junior, F., 2017. The Amazon at sea: Onset and stages of the Amazon River from a marine record, with special reference to Neogene plant turnover in the drainage basin. Global and Planetary Change 153, 51 – 65.

Horton, B.K., 2018. Tectonic regimes of the central and Southern Andes: Responses to variations in plate coupling during subduction. Tectonics 37, 402-429.

IBFN (International Big Fish Network), 2005. Surface currents of the Atlantic Ocean. www.bigmarineefish.com/map_currents_atlantic.jpg

Koutsoukos, E.A.M., 1982. Geohistória e paleoecologia das bacias marginais de Florianópolis e Santos. Congresso Brasileiro de Geologia 32, 2369-2382.

Kowsmann, R.O., Costa, M.P.A., 1974. Interpretação de testemunhos coletados na margem continental brasileira durante a operação GEOMAR VI. Simpósio de Oceanografia e Geologia Marinha, Porto Alegre.

Laprida, C., Chapori, N.G., Chiessi, C.M., Violante, R.A.,Watanabe, S., Totah, V., 2011. Middle Pleistocene Sea surface temperature in the Brazil-Malvinas Confluence Zone: Paleoceanographic implications based on planktonic foraminifera. Micropaleontology 57 (2), 183–195.

Lee, E.Y., Wagreich, M., 2018. Basin modelling with a MatLab-based program, BasinVis 2.0: A case study on the Southern Vienna Basin, Austria. Journal of the Geological Society of Korea 54 n. 6, 615-630.

Lee, E. Y., Novotny, J., Wagreich, M., 2019. Subsidence Analysis and Visualization for Sedimentary Basin Analysis and Modelling. Springer. SpringerBriefs in Petroleum Geoscience & Engineering. Cham, Switzerland. 56 pp. https://doi.org/10.1007/978-3-319-76424-5

Livermore, R., Nankivell, A., Eagles, G., Morris, P. 2005. Paleogene opening of the Drake Passage. Earth and Planetary Science Letters 236, 459-470. 10.1016/j.epsl.2005.03.027

Livermore, R., Hillebrand C.D., Meredith, M., Eagles, G., 2007. Drake Passage and Cenozoic climate: An open and shut case? Geochemistry Geophysics Geosystems 8, 1.

Martins, L.R., Urien, C.M., Butler, L.W., 1972. Províncias fisiográficas e sedimentos da margem continental atlântica. Congresso Brasileiro de Geologia, Belém-Pará.

MCNeill, L.C., Dugan, B., Backman, J., Pickering, K.T., Pouderoux, H.F.A., Henstock, T.J., Petronotis, K.E., Carter, A., Chemale Junior, F., Milliken, K.L., Kutterolf, S., Mukoyoshi, H., Chen, W., Kachovich, S., Mitchison, F.L., Bourlange, S., Colson, T.A., Frederik, M.C.G., Guerin, G., Hamahashi, M., House, B.M., Hupers, A., Jeppson, T.N., Keningsberg, A.R., Kuranaga, M., Nair, N., Owari, S., Shan, Y., Song, I., Torres, M.E., Vanucchi, P., Vrolijk, P.J., Yang, T., Zhao, X., Thomas, E., 2017. Understanding Himalayan erosion and the significance of the Nicobar Fan. Earth and Planetary Science Letters 475, 134 – 142.

Miller, D.J., Ketzer, J.M.M., Viana, A.R., Kowsmann, R.O., Freire, A.F.M., Oreiro, S.G., Augustin, A.H., Lourega, R.V., Rodrigues, L.F., Heemann, R., Preissler, A.G., Machado, C.X., Sbrissa, G.F. 2015. Natural gas hydrates in the Rio Grande Cone (Brazil): A new province in the western South Atlantic, Marine and Petroleum Geology 67, 187-196, https://doi.org/10.1016/j.marpetgeo.2015.05.012.

Mudelsee, M., Bickert, T., Lear, C.H., Lohmann, G., 2014. Cenozoic climate changes: A reviewed based on times series analysis of marine benthic δ18O records. Reviews of Geophysics 52, 333-374.

Müller, R.D., Sdrolias, M., Gaina, C., Roest, W.R., 2008. Age, spreading rates, and spreading asymmetry of the world's ocean crust. Geochemistry Geophysics Geosystems 9, n. 4.

Müller R.D., Seton, M., Zahirovic, S., Williams, S.E., Matthews, K.J., Wright, N.M., Shephard, G.E., Maloney, K.T., Barnett-Moore, N., Hosseinpour, M., Bower, D.J., Cannon, J., 2016. Ocean basin evolution and global-scale plate reorganization events since Pangea breakup, Annual Review of Earth and Planetary Sciences, Vol 44, 107-138. DOI: 10.1146/annurev-earth-060115-012211.

Perez-Diaz, L. and Eagles, G., 2014. Constraining South Atlantic Growth with Seafloor Spreading Data. Tectonics 33, 1848-1873. https://doi.org/10.1002/2014TC003644

Perez-Diaz, L., Eagles, G., 2017. A new high-resolution seafloor age grid for the South Atlantic. Geochemistry, Geophysics, Geosystems 18 (1), 457-470.

Perez-Diaz, L., Eagles, G., Sigloch, K. 2020. Indo-Atlantic plate accelerations around the Cretaceous-Paleogene boundary: A time-scale error, not a plume-push signal. Geology 48 (12): 1169–1173.

Potter, P.E., Szatmari, P., 2009. Global Miocene and the modern world. Earth-Science Reviews 96, 279-295.

Quade, J., Dettinger, M.P., Carrapa, B., DeCelles, P., Murray, K.E., Huntington, K.W., Cartwright, A., Canavan, R.R., Gehrels, G., and Clementz, M., 2015. The growth of the central Andes, 22°S–26°S, in: DeCelles, P.G., Ducea, M.N., Carrapa, B., Kapp, P.A. (Eds.), Geodynamics of a Cordilleran Orogenic System:

The Central Andes of Argentina and Northern Chile. Geological Society of America Memoir 212.

Ramos, V.A., 2009. Anatomy and global context of the Andes: main geologic features and the Andean orogenic cycle, in: Kay S.M., Ramos V.A., Dickinson W. (Eds.), Backbone of the Americas. Geological Society of América Memoir, GSA, Boulder 404, 31–65.

Ramos, V.A., 2010. The tectonic regime along the Andes: Present-day and Mesozoic regimes. Geological Journal 45, 2-25.

Rebesco, M., Hernandes-Molina, F.J., Van Rooij, D., Wahlin, A., 2014. Contourites and associated sediments controlled by deepwater circulation processes: State-of-art and future considerations. Marine Geology 352, 111-154.

Rizzi, M. A. M., Dillenburg, S. R., Takehara, L., Girelli, T. J., Lana. C. C., Chemale Junior, F. 2022. Andean fingerprimt on placer sands from the southern Brazilian coast. Sedimentary Geology 428, 106061. https://doi.org/10.1016/j.sedgeo.2021.106061

Rosa, A.P., 2007. Interpretação sismo-estratigráfica da porção da Bacia de Pelotas que engloba o Cone de Rio Grande e a avaliação do seu potencial petrolífero. Universidade Estadual do Norte Fluminense, Macaé.

Santos, T. P., Lessa, D. O., Venancio, I. M., Chiessi, C. M., Mulitza, S., Kuhnert, H., Govin, A., Machado, T., Costa, K. B., Toledo, F., Dias, B. B., Albuquerque, A. L. S. 2017. Prolonged warming of the Brazil Current precedes deglaciations. Earth and Planetary Science Letters 463, 1-12.

Sclater, J. G. and Christie,P.A.P., 1980.Continental stretching: An explanation of the Post-Mid-Cretaceous subsidence of the central North Sea Basin. JGR Solid Earth 85(B7), 3711-3739. https://doi.org/10.1029/JB085iB07p03711

Seton, M., J. Whittaker, P. Wessel, R. D. Müller, C. DeMets, S. Merkouriev, S. Cande, C. Gaina, G. Eagles, R. Granot, J. Stock, N. Wright, S. Williams, 2014, Community infrastructure and repository for marine magnetic identifications,Geochemistry, Geophysics, Geosystems, 5(4), 1629-1641, DOI:10.1002/2013GC005176

Serratt, H. 2021. Influence of SDR in the deposition of Pelotas Basin. Master Thesis, UNISINOS. São Leopoldo.50 pp.

Steckler, M. S. and Watts, A.B., 1978. Subsidence of the Atlantic-type continental margin off New York. Earth and Planetary Science Letters 41(1), 1-13 https://doi.org/10.1016/0012-821X(78)90036-5

Stica, J.M., Zalán, P.V., Ferrari, A.L., 2014. The evolution of rifting on the volcanic margin of the Pelotas Basin and the contextualization of the Paraná-Etendeka LIP in the separation of Gondwana in the South Atlantic. Marine and Petroleum Geology 50, 1-21.

Stramma, L. and England, M. 1999., On the water masses and mean circulation of the South Atlantic Ocean. Journal of Geoph. Res. 104 (C9), 20863-20883.

Urien, C.M., Martins, L.R., Martins I.R., 1978. Modelos deposicionales en la plataforma continental do Rio Grande do Sul, Uruguay y Buenos Aires. Introduction a los deltas ore-holocenos em la Terraza Continental Del Rio de La Plata. 7th Congresso Geologico Argentino, Argentina.

Watts, A.B., Ryan, W.B.F., 1976. Flexure of the lithosphere and continental margin basins. Tectonophysics 36, 25–44. https://doi.org/10.1016/0040-1951(76)90004-4

Wright J.D., 2009. Cenozoic Climate Change, in: Gornitz V. (Ed.) Encyclopedia of Paleoclimatology and Ancient Environments. Encyclopedia of Earth Sciences Series. Springer, Dordrecht

Zachos, J.C., Dickens, G.R., Zeebe, R.E., 2008. An early Cenozoic perspective on greenhouse warming and carbon-cycle dynamics. Nature 451, n. 17, 279-283.

Zalan, P.V. 2005. End members of gravitational fold and thrust belts (GBTFs) in the deep waters of Brazil. In: Shaw, J.H., Connors, C., Suppe, J. (Eds.), Seismic interpretations of contrational fault-related folds, vol. 53. AAPG Memoir, pp. 147–153.

Zhang, Y.P., Pagani, M., Liu, Z., Bohaty, S.M., DeConto, R., 2013. A 40-million-year history of atmospheric CO2. Philosophical Transactions of the Royal Society 371.

Zouain, R.N.A.,1986. Aspectos da dinâmica sedimentar no Rio de La Plata na porção exterior e na plataforma interna adjacente. Universidade Federal do Rio Grande do Sul, Porto Alegre.

Supplementary Material SM1

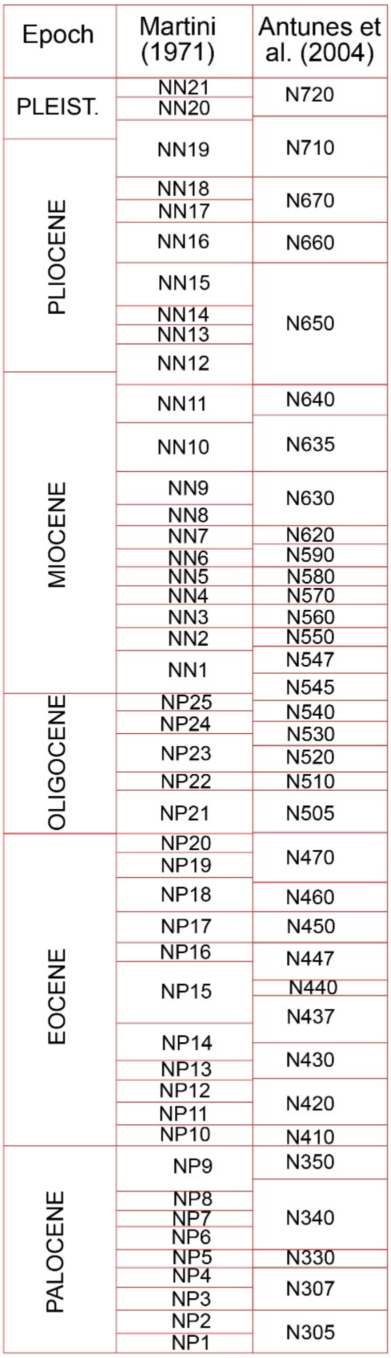

Epoch	Martini (1971)	Antunes et al. (2004)
PLEIST.	NN21	N720
	NN20	
PLIOCENE	NN19	N710
	NN18	N670
	NN17	
	NN16	N660
	NN15	N650
	NN14	
	NN13	
	NN12	
MIOCENE	NN11	N640
	NN10	N635
	NN9	N630
	NN8	
	NN7	N620
	NN6	N590
	NN5	N580
	NN4	N570
	NN3	N560
	NN2	N550
	NN1	N547 N545
OLIGOCENE	NP25	N540
	NP24	N530
	NP23	N520
	NP22	N510
	NP21	N505
EOCENE	NP20	N470
	NP19	
	NP18	N460
	NP17	N450
	NP16	N447
	NP15	N440 N437
	NP14	N430
	NP13	
	NP12	N420
	NP11	
	NP10	N410
PALOCENE	NP9	N350
	NP8	N340
	NP7	
	NP6	
	NP5	N330
	NP4	N307
	NP3	
	NP2	N305
	NP1	

Biozonation of calcareous nannofossils from the Brazilian margin of Antunes et al., (2004) correlated with international biozonation of calcareous nannofossils by Martini (1971).

Supplementary Material SM2

	1-RSS-3-RS	1-RSS-2-RS	2-RSS-1-RS	1-SCS-2-SC	1-SCS-3B-SC
N720	Shale	Shale	Shale	Shale	Shale
N710					
N670	Shale	Shale	Shale	Shale	Shale
N660					
N650		Shale	Shale	Shale	Shale
N640	Shale	Shale	Shale	Shale	Shale
N635					
N630	Shale	Shale	Shale	Shale	Shale
N620					
N590	Shale	Shale	Shale	Shale	Shale
N580	Shale	Shale	Shale	Shale	Shale
N570	Fine Sandstone	Shale	Shale	Shale	Shale
N560	Shale	Shale	Shale	Coarse sandstone	Shale
N550			Shale	Shale	Shale
N547					
N545					
N540			Shale	Shale	Shale
N530			Shale	Shale	Shale
N520	Fine Sandstone		Shale		Shale
N510	Fine Sandstone	Fine Sandstone	Shale	Fine Sandstone	
N505					
N470			Shale	Shale	Shale
N460	Fine Sandstone	Fine Sandstone	Shale	Shale	Shale
N450	Fine Sandstone	Fine Sandstone	Shale	Shale	Shale
N447					
N440					
N437					
N430			Shale		Shale
N420	Fine Sandstone	Fine Sandstone	Shale		Shale
N410			Shale	Shale	Shale
N350		Shale	Shale		
N340					

Lithological log

III. Manuscrito 2

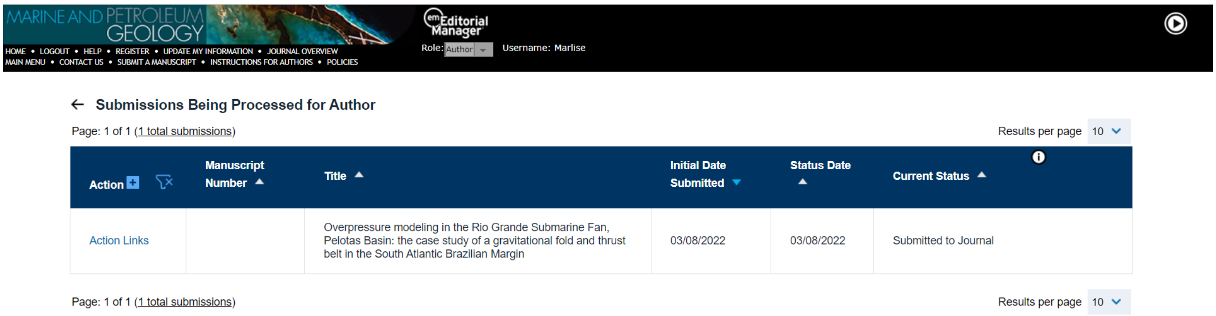

Username: Marlise

Submissions Being Processed for Author

Page: 1 of 1 (1 total submissions)

Results per page 10

Action	Manuscript Number	Title	Initial Date Submitted	Status Date	Current Status
Action Links		Overpressure modeling in the Rio Grande Submarine Fan, Pelotas Basin: the case study of a gravitational fold and thrust belt in the South Atlantic Brazilian Margin	03/08/2022	03/08/2022	Submitted to Journal

Page: 1 of 1 (1 total submissions)

Results per page 10

Overpressure modeling in the Rio Grande Submarine Fan, Pelotas Basin: the case study of a gravitational fold and thrust belt in the South Atlantic Brazilian Margin

Marlise Colling Cassel*[1], Marcelo Ketzer[2], Marcus Vinicius Aparecido Gomes de Lima[3], Farid Chemale Jr. [1]

[1]Vale do Rio dos Sinos University, Geology Graduate Program, Av. Unisinos, 950, São Leopoldo, Rio Grande do Sul, CEP 93022-000, Brazil

[2]Linnaeus University, Department of Biology and Environmental Sciences, 391-82, Kalmar, Sweden

[3]Universidade Federal do Pampa, Campus Caçapava do Sul, Caçapava do Sul, Brazil

*Corresponding author: Marlise Colling Cassel (marlise.cassel@gmail.com)

Abstract

Overpressure in sedimentary basins is a phenomenon potentially linked to geohazards, existence of hydrocarbons, and key to unravel passive margins evolution. Its occurrence can be caused by autochthonous and allochthonous factors such as regional tectonics, undercompaction due to high sedimentation rate, clay transformation, and hydrocarbon generation. In the Brazilian South Atlantic margin, the Rio Grande Submarine Fan is a well-known large-scale fanlike feature on the continental slope, presenting a complex structural setting caused by gravitational collapse along a detachment surface. This feature provides a natural laboratory to study overpressure generation. This study aims to investigate, for the first time quantitatively, the overpressure occurrence in the Rio Grande Submarine Fan. Basin numerical modeling of temprerature and overpressure was performed using seismic and well data obtained from the National Agency for Petroleum, Natural Gas and Biofuels (ANP) and the TemisFlow suite. The results provide crucial information on the dimension, intensity of the overpressure zone, autochthonous and allochthonous processes, and factors for the overpressure occurrence. The current temperature and overpressure configuration ranges from 6°C to 151°C and 0 MPa to 39 MPa, presenting a topward values decrease, except near the detachment zone where abrupt changes occur. Deposition of dominantly fine-grained sediments under high sedimentation rates and clay transformations, Andean tectonism, and oceanic currents patterns play a significant role to development of the overpressure, as well as the gravitational collapse of the Rio Grande Submarine Fan.

Keywords: numerical modeling; passive margin; clay transformation; undercompacted shale; detachment

1. Introduction

Fluid overpressure is an important phenomenon for understanding continental margins evolution, hydrocarbon exploration, and geohazards (Morley et al., 2011, Reis et al., 2016, Souza et al., 2020). In deep marine environments, overpressure is an important triggering mechanism for mass transport, which rework previous sedimentary deposits and activate sin-sedimentary faults (Bolton et al., 1998). Overpressure is defined as any pore pressure that exceeds the hydrostatic pressure in the sedimentary column. Consequently, it changes the sediment strength, and potentially helps destabilization of the sedimentary package leading to gravitational collapse (Dickinson, 1953). Overpressure may be originated by autochthonous or allochthonous processes to the system, including regional tectonics, undercompaction due to high sedimentation rate, clay transformation, and hydrocarbon generation (Law et al., 1983; Bruce, 1984; Burrus, 1998; Swarbrick and Osborne, 1998; Law and Spencer, 1998; Grauls, 1999, Souza et al, 2020). Overpressure is commonly associated with large depocenters in deepwater settings. It may be an essential feature to weaken the sedimentary package and cause the downslope gravitational collapse of thick, fine-grained sequences lacking salt deposits (Rowan et al., 2004).

There is a large-scale fanlike feature on the continental slope of the Brazilian South Atlantic margin called Rio Grande Submarine Fan (RGF; Martins et al 1972, Miller et al., 2015). It consists of a thick (4 km) mud and shale package, deposited since the Miocene (Fontana, 1996, Abreu, 1998, Rosa, 2007, Anjos-Zerfass et al., 2014, Chemale Jr. et al., 2021). RGF has characteristics related to overpressure: a large proportion of fine-grained sediments, possible hydrocarbon generation, and a high sedimentation rate (Anjos-Zerfass et al., 2014). Additionally, previous studies about the RGF structural setting show different structural features related to gravity tectonics, including a basal detachment surface and an upper slope extensional and lower slope compressional domains (Fontana, 1996, Abreu, 1998, Zalan, 2005, Rosa, 2007, Anjos-Zerfass et al., 2014, Chemale Jr. et al., 2021). In the case of a fine-grained siliciclastic package, like the RGF, the cause for the gravitational collapse above the detachment surface is poorly constrained. Overpressured shales such as in the Amazon Fan induce such process (Cobbold et al., 2004; Oliveira, 2005; Perovano et al., 2011, Souza et al., 2020). However, the existence, distribution, and magnitude of the overpressure in the RGS is still speculative.

This paper aims to investigate the overpressure occurrence in the RGF applying basin modeling techniques based on 2D exploration seismic sections and well data. For the first time, this study identifies the dimensions and intensity of the overpressured zone, and possible autochthonous and allochthonous processes involved on its development. This paper also considers the hypothesis that an overpressured zone weakened the sedimentary package, creating a detachment surface leading to gravitational collapse and the complex structural domains of the RGF. The results contribute to the understanding of overpressure occurrence and gravitational collapse of deep water depocenters, which have a direct impact on hydrocarbon exploration and geohazard risk assessment (Zalan, 2005, Reis et al., 2016, Souza et al., 2020).

2. Geological setting and study area

The RGF is located in the Pelotas Basin (Fig 1A e Fig 1B), on the southern Brazilian Atlantic passive margin, which resulted from the Gondwana breakup. This basin covers 250,000 km² and an emerged segment with an area of 40,000 km² constitutes a coastal plain (Anjos-Zerfass, 2009). The Pelotas Basin is limited to the north by the Santos Basin through the Rio Grande Fracture Zone (Fig. 1A). The southern limit is the Polonio High, separating the Pelotas Basin from the Punta del Este Basin (Stica et al., 2014) (Fig. 1A). The thickness of the basin reaches up to 12 km from Barremian to Recent. According to Bueno et al. (2007), clastic fans and deltas spread over the distal deposits from the Oligocene onwards, forming a large regressive sedimentary wedge in the Neogene (Fig. 1C). In this context of increased sedimentary input, the RGF formation took place, which still has aspects related to its genesis under discussion (Abreu, 1998, Bueno et al., 2007, Rosa, 2007, Chemale et al, 2021).

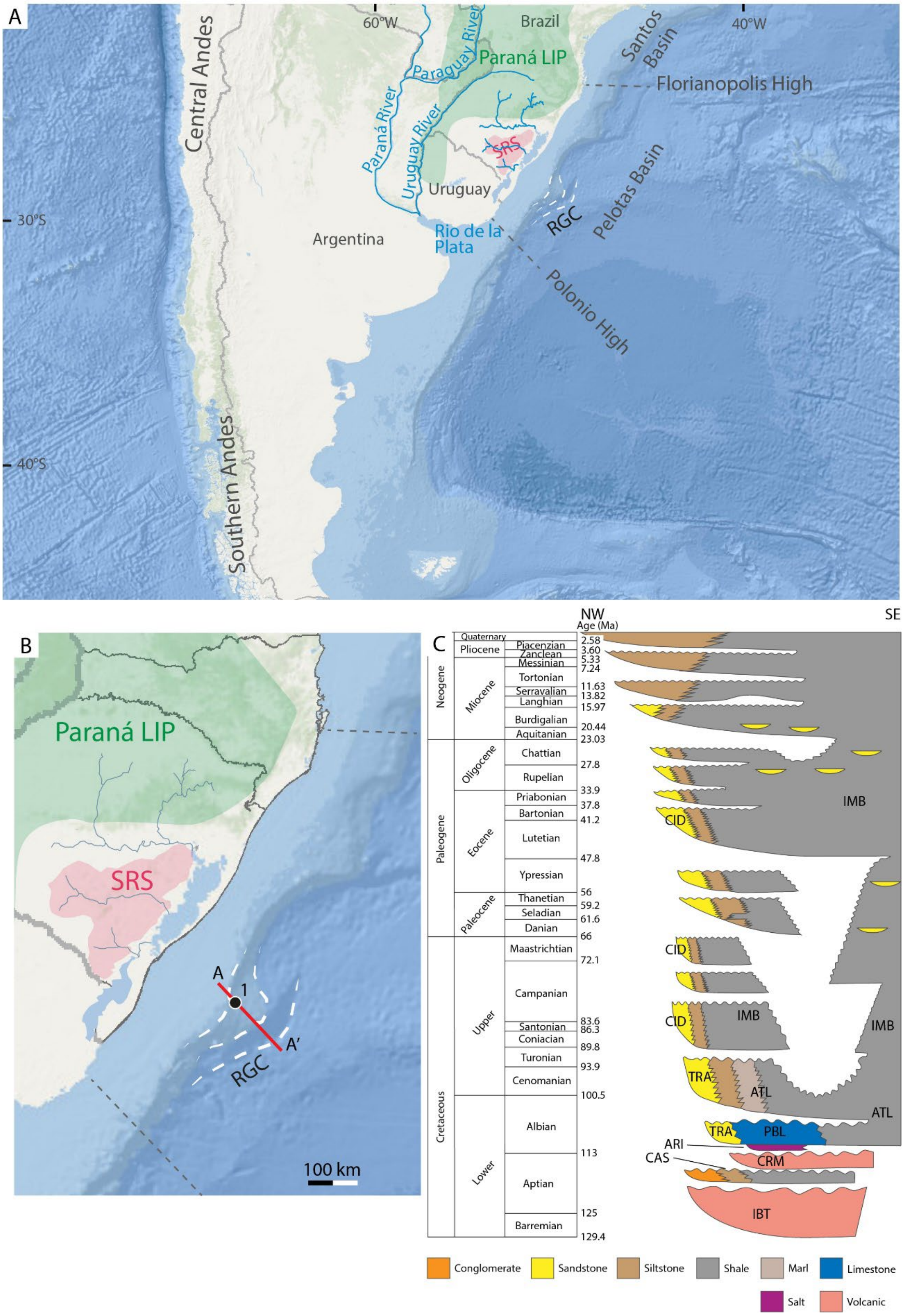

Figure 1. Study area and geological context. A) Map of southern South America showing the main structures on land and in the southern Atlantic Ocean and the location of the Pelotas Basin with its northern and southern limits (dashed grey

lines). Areas: SRS = Sul-Riograndense Shield; RGF = Rio Grande Submarine Fan, highlighted by white dashed lines. B) Map of the Pelotas Basin with interpreted seismic section (A-A’ = J99B194) and well (1 = 1BRSA61RSS). C) Chronostratigraphic chart of the Pelotas Basin adapted from Bueno et al. (2007). Formations: IBT = Imbituba, CAS = Cassino, CRM = Curumim, ARI = Ariri, PBL = Porto Belo, TRA = Tramandaí, ATL = Atlântida, CID = Cidreira, IMB = Imbé.

The RGF is a large-scale fanlike feature in the Pelotas Basin continental slope and is the main depocenter since the Miocene (Martins et al 1972 Miller et al., 2015) (Fig. 1B). The sedimentation consists of a thick mud and shale package. Two main sediment sources are considered for the RGF: a) the Rio de la Plata River, which contributes with distal fine sediments of Andean Cordillera (Chemale Jr. et al., 2021), transported by contour currents existing in the north and south of the Pelotas Basin (Wilckens et al., 2021, Viana, 2001) b) and sediments from the Rio Grande do Sul and Uruguay rocks (crystalline basement and Phanerozoic sedimentary and volcanic rocks) (Martins et al., 1972; Urien et al., 1978; Zouain, 1986; Castillo-López, 2009).

The RGF shows a complex structural setting, concentrated in different domains, connected at the base by a detachment surface (Fontana, 1996, Abreu, 1998, Zalan, 2005, Bueno et al, 2007, Rosa, 2007) (Fig 2A). The detachment surface triggered a gravitational collapse and consequently gravitational fold and thrust belt (GFTB) (Zalan, 2005). The distal structural domain is compressive and corresponds to this GFTB. The proximal domain is distensive and corresponds to normal listric faults (Fontana, 1996, Abreu, 1998, Zalan, 2005, Rosa, 2007). Additionally, these authors speculated about shale overpressure as the main mechanism responsible for nucleating a rupture along the detachment surface.

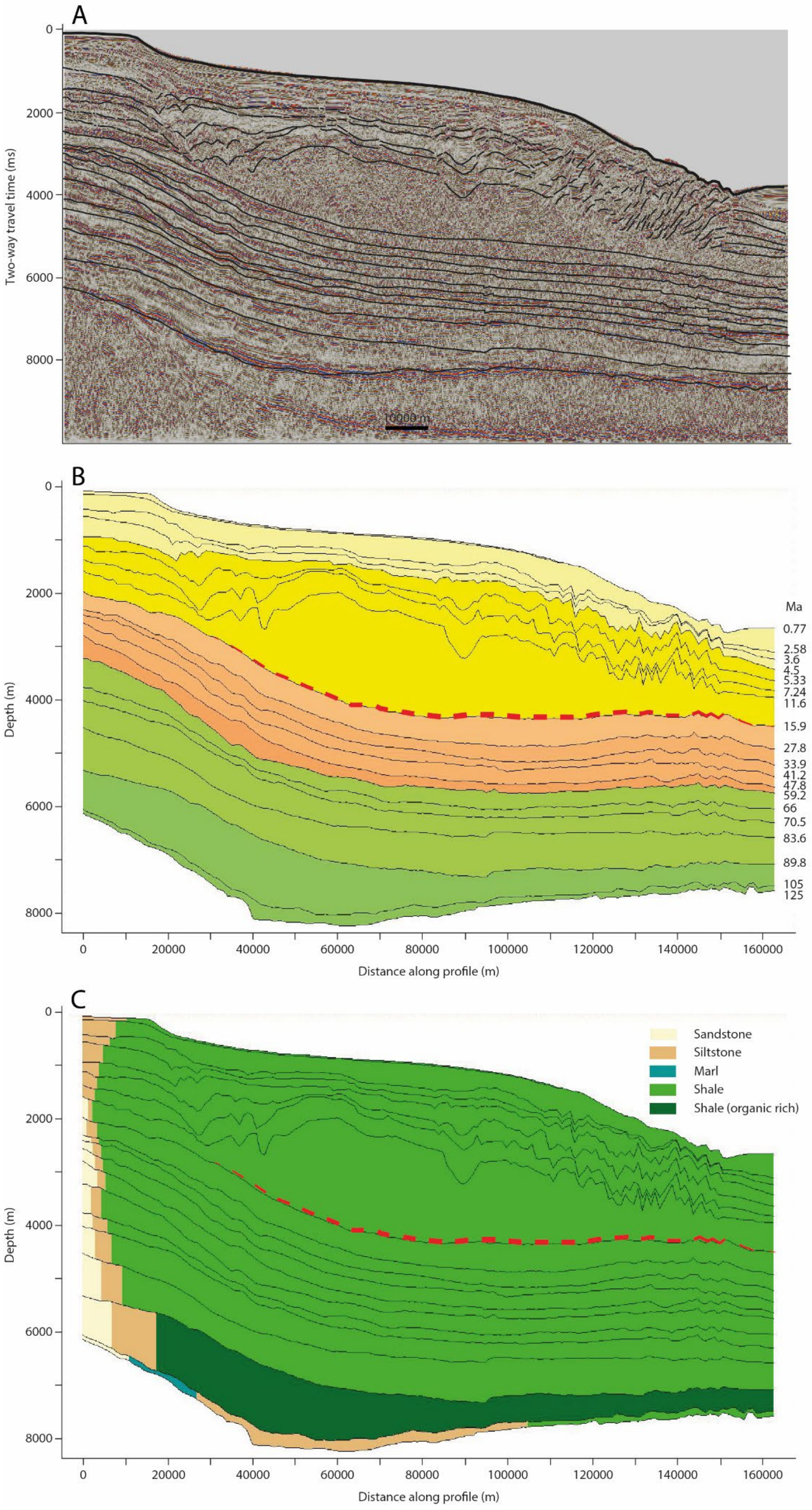

Figure 2. A) Interpreted seismic line in two-way time, where the colored lines

indicate stratigraphic surfaces described in Rosa (2007) and the red-black dashed line indicates the RGF basal detachment surface, modified from Rosa (2007). Above the basal surface, the RGF displays different structural domains, where the proximal portion corresponds to distensive listric faults. In contrast, the distal portion corresponds to compressive gravitational fold and thrust belt. B) The stratigraphic framework (according to Rosa, 2007), in depth, highlighting the detachment surface in the red dashed line. C) Main lithologies (according to Bueno et al., 2007), in depth, highligting the detachment surface in the red dashed line.

3. Data and methods

This study is based on exploration data obtained from the National Agency for Petroleum, Natural Gas and Biofuels (ANP), comprising a multichannel reflection seismic section calibrated with well data (Fig. 1B). These data were analyzed through seismic interpretation, time-depth conversion, and overpressure modeling.

3.1 Seismic data

The profile analyzed in this study crosses the central portion of the RGF in the dip direction NW-SE (Fig. 1B). The profile is 160300 m long and 11000 ms in two-way travel time (TWTT) (Fig. 2A). For this study, the seismic section interpretation followed the detailed stratigraphic framework of Rosa (2007) (Fig 2B).

3.2 Well data

This study used well data (Fig. 1B) for the time-depth conversion of the horizons present in the seismic section. The time-depth conversion required an interpreted seismic section that intersects an well (Well 1, Fig. 1B). These steps are detailed in subsequent items.

3.3 Time-depth conversion

The time-depth conversion of the interpreted seismic horizons considered the travel time equation of the vertically reflected seismic wave (Equation 1):

Depth = (average velocity) × (two-way time/2)

Where two-way time is the horizon time interpreted in the zero-offset section, and average velocity is the velocity profile obtained from Well 1 vertical seismic profile (VSP).

3.4 2D Basin modelling

The 2D basin modeling was executed in the TemisFlow Petroleum System Software (IFPen – French Institute of Petroleum, version 2019). The first step was to import the horizons (previously converted to depth). Afterward, each horizon received an age, following the stratigraphic framework of Rosa (2007) (Fig. 2B). After that each interval between the horizons received lithologies, according to Bueno et al. (2007) and Rosa (2007) (Figure 2C).

For overpressure modeling, variables such as porosity, permeability, and sedimentation rate were computed. The porosity and permeability variables used in this modeling were extracted from the IFPen Lithology Library and the sedimentation rate variable was calculated by restoring past geometries. TemisFlow performs this function through the backstripping technique based on current geometry and lithofacies compaction laws.

The next step was parameterizing the temperature conditions. The computation of the temperature distribution resulting from the heat transfer through the sedimentary basin requires the definition of a thermal basement. The options available in TemisFlow for thermal regimes computation include geothermal gradients, heat flow at base sediments, heat flow at the base upper mantle. Based on available well data (Well 1, Fig. 1B), the model ran with 20°C/km as thermal gradient and seafloor temperature varing from 6 °C (shallow water) to 3°C (deep water at 13600 m), according to Ketzer et al. (2020).

4. Results

4.1 2D basin modeling: temperature

The current temperature configuration ranges from 6°C to 151°C (Fig 3). The highest temperature occurs in the lower intervals and decreases towards the upper intervals. In general, this change occurs gradually.

However, this pattern is different in the central area of the model near the base of the RGF, at 3800 m depth. Around this area, the temperature changes abruptly. Below 3800 m depth in the section's central part, the temperature is nearly constant (ca. 90°C) since 5600 m depth. At 3800 m depth, a temperature contrast of 100% occurs. The upper interval with a temperature of 50°C is in contact with the lower interval of 100°C.

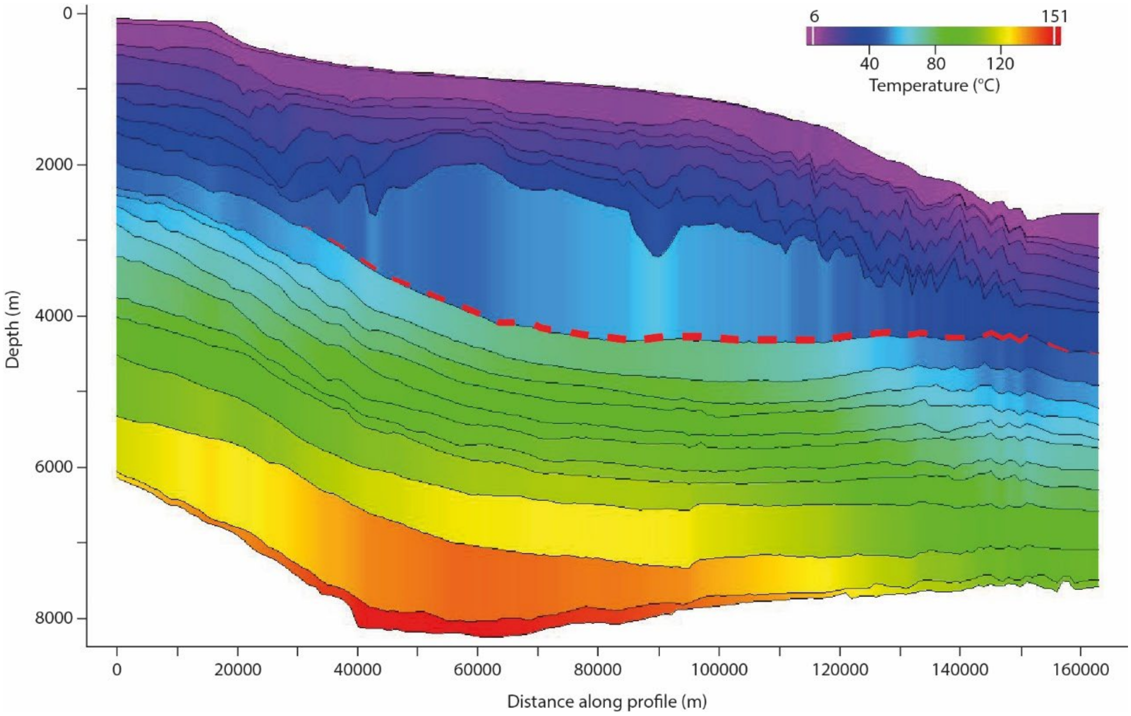

Figure 3. Result of temperature modeling along a section at the present day. The detachment surface (red dashed line) coincides with a temperature contrast and interrupts the gradual upward reduction of temperature at the central portion of the section.

4.2 2D basin modeling: overpressure

The current overpressure configuration ranges from 0 MPa to 39 MPa, and its variation distribution follows two patterns (Fig. 4): a) low overpressure occurs in the upper intervals and also in the proximal portion of the section (reaching up to 1000 m to 1700 m of distance from the beginning of the line) since the basal intervals. b) In the remaining section the higher overpressure occurs in the lower intervals and decreases towards the upper intervals. In general, this change occurs gradually.

However, this pattern is different in the central part of the model, at 3800 m depth, just like the temperature. Around this area, between 60000 m and 120000 m of distance from the beginning of the line, the overpressure changes abruptly. Below 3800 m in the section's central part, the overpressure is constant since 4800 m depth. At 3800 m, a pressure difference of 90% occurs, where the upper interval with a overpressure of 14 MPa is in contact with the lower interval with a overpressure of 26 MPa. Besides, at intermediate depth, a lateral temperature variation also occurs, with a higher value in the center.

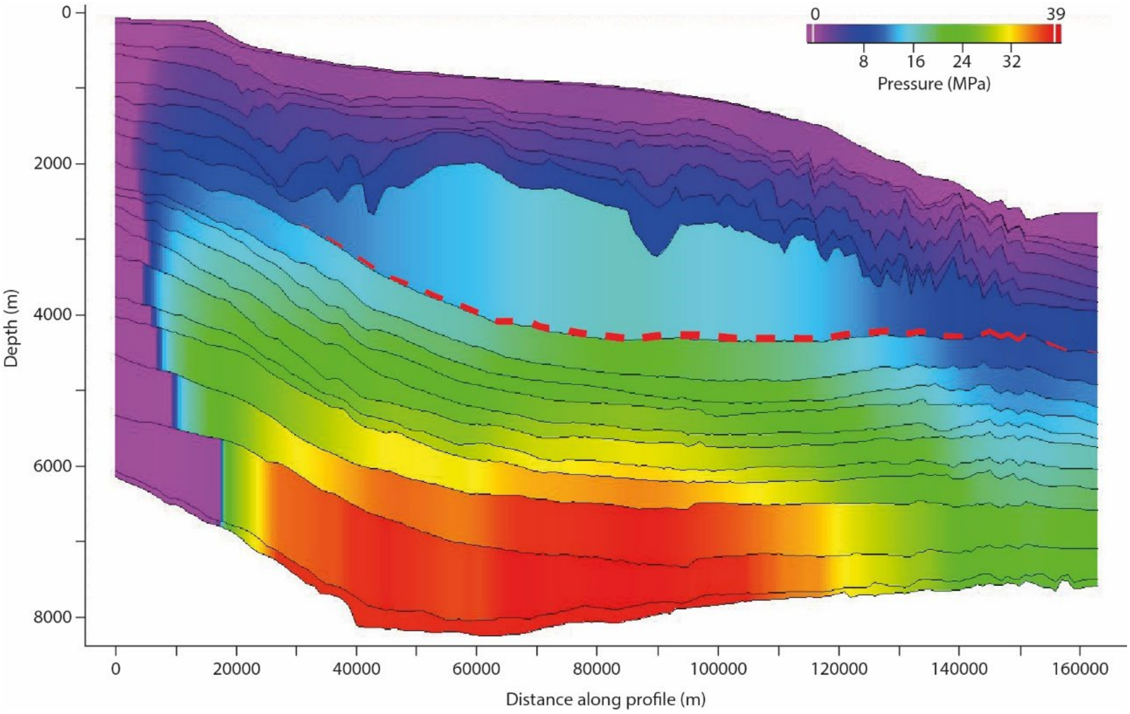

Figure 4. Result of overpressure modeling along a section at the present day. The detachment surface marks a overpressure contrast and interrupts the gradual change to lower overpressure towards the upper intervals in the central portion of the section. Additionally, the lower overpressure occurs in the proximal portion of the section.

5. Discussion

5.1 Overpressure, detachment and gravitational collapse

Previous authors (Fontana, 1996, Abreu, 1998, Zalan, 2005, Rosa, 2007) described and documented the complex structural arrangement of the RGF resulting from gravitational collapse and its relation to a basal detachment surface. Additionally, these authors speculated about shale overpressured as the main mechanism responsible for nucleating a rupture along a detachment surface. This information is qualitatively supported by: *a)* lithology of the package, which is predominantly composed of shales and clays and *b)* high sedimentation rate. However, although the existence of such overpressure has been indicated with the evidence above, there is no well or modelling data to further support and quantify it.

The results of the 2D basin modeling of overpressure in the analyzed section consist of the first quantitative direct evidence of the overpressure occurrence in the RGF. The overpressure occurs from the base of the section and presents an abrupt change in overpressure values below and above the basal detachment surface (Fig. 4). Thus, the results presented in the modeling agree with previous speculations and confirm the existence of overpressure at the base of the RGF.

In addition to the two factors mentioned above (*a)* dominantly fine-grained sedimentary package and *b)* high sedimentation rate) that could contribute to the formation of overpressure, the hydrocarbon generation and smectite-illite transformation can also play an important role in creating fluid overpressure (Bruce, 1984, Souza et al., 2020). However, since this study followed the stratigraphic framework of Rosa (2007) (Fig. 2A) where faults do not directly connect the Turonian source rock with deposits at the detachment surface, it is possible to assume that hydrocarbon generation and migration is not a major mechanism to overpressure development in the RGF. Regarding the smectite-illite transformation contribution, the temperature modeling results (Fig. 3) show that the section area close to the detachment reaches temperatures belonging to the transformation window, 70 – 150 °C (Bruce, 1984).

The modeling results associated with previous literature data allow delimit the RGF generating overpressure factors. Thus, there are three main causes for the overpressure and consequent detachment and gravitational collapse in the RGF: *a)* a considerable package of undercompacted shale (4300 m thick), *b)* high sedimentation rate, and *c)* smectite-illite transformation.

However, it is still possible to discuss the characterization of the detachment surface. The RGF overpressure detachment surface occurs above the zone of greatest overpressure reported at the base of the section. This occurs when the gravitational stress relief (which tends to occur where there sediment strenght decreases, in this case due to overpressure) is sustained by lithostatic pressure. Thereby, the gravitational tension is released in the plane where the overpressure exceeds the lithostatic pressure, tending to occur topwards, as the lithostatic pressure decreases (Fossen, 2010). Additionally, the detachment occurs along a regional surface in the Pelotas Basin, which is related to allochtonous factors (Cassel et al, 2022).

5.2 Allochthonous and autochthonous factors

Mechanisms generating overpressure can be classified between allochthonous or autochthonous. The allochthonous mechanisms are related to external factors, whilst autochthonous are related to an increase in internal fluid content (Souza et al., 2020). Regional tectonics and undercompactation are examples of allochthonous factors, whereas clay transformation and hydrocarbon generations are exemples of autochthonous factors.

In the case of RGF, this study and previous authors (Zalan, 2005, Rosa, 2007) show three causes for overpressure: *a)* a huge package of undercompacted shale (4300 m thick), *b)* high sedimentation rate and *c)* smectite-ilite transformation. The temperature modeling showed values within the smectite-ilite transformation window, as discussed in the previous item. This factor, which causes an increase in the internal fluid content, is autochthonous and results from the thermal gradient in the case of RGF. The other two causing factors of overpressure are allochthonous. External controls are related to the deposition of a considerable shale package (4300 m thick), enhanced by the high sedimentation rate.

The origin of RGF deposition and the sedimentation pattern are associated with the Andean mountains uplift pulses, Drake Passage widening pulses, and consequent Antarctic Circumpolar Current (Cassel et al, 2022). This context led to the occurrence of a relevant basin unconformity which correspond to a regional surface in the Pelotas Basin, and influenced the RGF shale deposition enhanced by the high sedimentation rate. Since the detachment occurs along this regional surface these allochthonous controls influence not only de sedimentation pattern, but also the detachment surface. Consequently, the allochtonous factors for the overpressure and consequent are triggered by regional events associated with Andean mountain uplift and Drake Passage widening.

6. Conclusion

For the first time, this study investigated the occurrence and main mechanisms of overpressure, which contributed to the gravitational collapse of the Rio Grande Submarine Fan. It was performed based on basin numerical modeling of temperature and overpressure, using exploration data obtained from the National Agency for Petroleum, Natural Gas and Biofuels (ANP), comprising a multichannel reflection seismic section, calibrated with well data.

The modeling results indicate that the overpressure in the RGF explains the detachment surface and gravitational collapse. The maximum overpressure value reaches 39 Mpa at the bottom and tends to decrease upwards. But at intermediate depths (3800 m), corresponding to the detachment surface, occurs an abrupt contrast of 90% of the value (from 26 Mpa to 14 Mpa). The temperature tends to vary gradually from 151 °C at the bottom to 6 °C at the top. But also in the detachment surface a 100% contrast change occurs in the values.

The modeling results previous literature delimit the RGF generating overpressure causes: *a)* a huge package of undercompacted shale (4300 m thick), *b)* high sedimentation rate, and *c)* smectite-illite transformation. These factors were classified between allochthonous (a and b) and autochthonous (c). The autochthonous one is controlled by temperature. The allochthonous are associated with the Andean mountain's uplift pulses and Drake Passage widening pulses.

Acknowledgments

This project has been supported by UNISINOS-PETROBRAS Cooperation Agreement (#5900.0109881.18.9). The authors thank the Brazilian Agency of Petroleum, Natural Gas and Biofuels (ANP) for the data availability. Marlise Colling Cassel is grateful to Coordination for the Improvement of Higher Education Personnel (CAPES) for the Ph.D. scholarship and for the Linneuniversitetet for welcoming as PhD Exchange Student.

References

Abreu, V.S.,1998. Geologic Evolution of conjugate volcanic passive margins: Pelotas Basin (Brazil) and offshore Namibia (Africa) Implication for global sea-level changes. Rice University, Houston.

Anjos-Zerfass, G.S., Souza, P.A., Chemale Jr., F., 2008. Biocronoestratigrafia da Bacia de Pelotas: estado atual e aplicação na geologia do petróleo. Revista Brasileira de Geociências 38, 47-62.

Bolton, A.J., Maltman, Alex, Clennell, M., 1998. The importance of overpressure timing and permeability evolution in fine-grained sediments undergoing shear. J. Struct. Geol. 20, 1013–1022. https://doi.org/10.1016/S0191-8141(98)00030-3.

Bruce, C.H., 1984. Smectite dehydration – its relation to structural development and hydrocarbon accumulation in northern Gulf of Mexico basin. AAPG (Am. Assoc. Pet. Geol.) Bull. 68, 673–683.

Bueno, G.V., Zacharias, A.A., Oreiro, S.G., Cupertino, J.A., Falkenhein, F.U.H., Neto, M.A., 2007. Bacia de Pelotas. Boletim de Geociências da Petrobrás 15, n. 2, 557-559.

Burrus, J., 1998. Overpressure models for clastic rocks, their relation to hydrocarbon expulsion: a critical reevaluation. In: Law, B.E., Ulmishek, G.F., Slavin, V.I. (Eds.), Abnormal Pressures in Hydrocarbons Environments, vol. 70. AAPG Memoir, pp. 35–63.

Castillo-López, L.A., 2009. Interpretação sismoestratigráfica e geomorfologia sísmica do Cone de Rio Grande, Bacia de Pelotas. Universidade Federal do Rio Grande do Sul, Porto Alegre.

Chemale Junior, F., Lavina, E.L.C., Carassai, J.J., Girelli, T.J., Lana, C., 2021. Andean orogenic signature in the Quaternary sandy barriers of Southernmost Brazilian Passive margin – Paradigm as a source area. Geoscience Frontiers 12(4),101119. https://doi.org/10.1016/j.gsf.2020.11.015

Cobbold, P.R., Mourges, R., Boyd, K., 2004. Mechanism of thin-skinned detachment in the Amazon Fan: assessing the importance of fluid overpressure and hydrocarbon generation. Mar. Petrol. Geol. 21, 1013–1025. https://doi.org/10.1016/j.marpetgeo.2004.05.003.

Dickinson, G., 1953. Geological Aspects of Abnormal Reservoir Pressures in Gulf Coast, vol. 61. AAPG Bulletin, Louisiana, pp. 2134–2142.

Fontana, 1996. Geotectônica e sismoestratigrafia da Bacia de Pelotas e Plataforma de Florianópolis. Doctorate thesis, Universidade Federal do Rio Grande do Sul, Porto Alegre, 216 p..

Fossen, H. 2010. Structural Geology. Cambridge University Press, Cambridge.

Grauls, D., 1999. Overpressure: causal mechanisms, conventional and hydromechanical approaches. Oil & Gas Sci. Technol. Rev. IFP 54 (6), 667–678.

Ketzer, J.M., Praeg, D., Rodrigues, L.F., Augustin, A., Pivel, M.A.G., Rahmati-Abkenar, M., Miller, D.J., Viana, A.R., Cupertino, J.A. 2020. Gas hydrate dissociation linked to contemporary ocean warming in the southern hemisphere. Nature Communications. 11 (1). 1-9.

Law, B.E., Hatch, J.R., Kukal, G.C., Keighin, C.W., 1983. Geological implications of coal dewartering. AAPG (Am. Assoc. Pet. Geol.) Bull. 67, 2250–2260.

Law, B.E., Spencer, C.W., 1998. Abnormal pressures in hydrocarbon environments. In: Law, B.E., Ulmishek, G.F., Slavin, V.I. (Eds.), Abnormal Pressures in Hydrocarbons Environments, vol. 70. AAPG Memoir, pp. 1–11.

Martins, L.R., Urien, C.M., Butler, L.W., 1972. Províncias fisiográficas e sedimentos da margem continental atlântica. Congresso Brasileiro de Geologia, Belém-Pará.

Miller, D.J., Ketzer, J.M.M., Viana, A.R., Kowsmann, R.O., Freire, A.F.M., Oreiro, S.G., Augustin, A.H., Lourega, R.V., Rodrigues, L.F., Heemann, R., Preissler, A.G., Machado, C.X., Sbrissa, G.F. 2015. Natural gas hydrates in the Rio Grande Cone (Brazil): A new province in the western South Atlantic, Marine and Petroleum Geology 67, 187-196, https://doi.org/10.1016/j.marpetgeo.2015.05.012.

Morley, C.K., King, R., Hillis, R., Tingay, M., Backe, G., 2011. Deepwater fold and thrust belt classification, tectonics, structure and hydrocarbon prospectively: a review. Earth Sci. Rev. 104 (1–3), 41–91. https://doi.org/10.1016/j.earscirev.2010.09.010.

Oliveira, V., 2005. A Tectônica Gravitacional do Cone do Amazonas: compartimentação estrutural e mecanismos controladores. Tese de Mestrado. Universidade Federal Fluminense

Perovano, R.J.S., Vendeville, B.C., Reis, A.T., Silva, C.G., Gorini, C., Araujo, E.F.S., 2011. Modelagem fisica experimental de mecanismos de dedormação gravitacional simulando multiplos intervalos superpressurizados: apliacação à Bacia da Foz do Amazonas. Rev. Bras. Geofís. 29 (3), 583–607.

Reis, A.T., Araújo, E., Silva, C.G., Cruz, A.M., Gorini, C., Droz, L., Migeon, S., Perovano, R., King, I., Bache, F. 2016. Effects of a regional décollement level for gravity tectonics on late Neogene to recent large-scale slope instabilities in the Foz do Amazonas Basin, Brazil, Marine and Petroleum Geology 75, 29-52. https://doi.org/10.1016/j.marpetgeo.2016.04.011.

Rosa, A.P., 2007. Interpretação sismo-estratigráfica da porção da Bacia de Pelotas que engloba o Cone de Rio Grande e a avaliação do seu potencial petrolífero. Universidade Estadual do Norte Fluminense, Macaé.

Rowan, M.G., Peel, F.J., Vendeville, B.C., 2004. Gravity-driven fold belts on passive margins. In: McClay, K.R. (Ed.), Thrust Tectonics and Petroleum System. AAPG Memoir, p. 82.

Souza, J.M.G, Cubas, N., Rabe, C., Letouzey, J., Divies, R., Praeg, D.B., Granjeon, D., Cruz, A.M, Silva, C.G, dos Reis, A.T., Gorini, C. 2020. Controls on overpressure evolution during the gravitational collapse of the Amazon deep-sea fan, Marine and Petroleum Geology 121, https://doi.org/10.1016/j.marpetgeo.2020.104576.

Stica, J.M., Zalán, P.V., Ferrari, A.L., 2014. The evolution of rifting on the volcanic margin of the Pelotas Basin and the contextualization of the Paraná-Etendeka LIP in the separation of Gondwana in the South Atlantic. Marine and Petroleum Geology 50, 1-21.

Swarbrick and Osborne, 1998. Mechanisms that generate abnormal pressures: an overview. In: Law, B.E., Ulmishek, G.F., Slavin, V.I. (Eds.), Abnormal Pressures in Hydrocarbon Environments, vol. 70. AAPG Memoir, pp. 13–34.

Viana, A.R. 2001. Seismic expression of shallow- to deep-water contourites along the south-eastern Brazilian margin. Marine Geophysical Researches 22, 509-521.

Urien, C.M., Martins, L.R., Martins I.R., 1978. Modelos deposicionales en la plataforma continental do Rio Grande do Sul, Uruguay y Buenos Aires. Introduction a los deltas ore-holocenos em la Terraza Continental Del Rio de La Plata. 7th Congresso Geologico Argentino, Argentina.

Wilckens, H., Miramontes, E., Schwenk, T., Artana, C., Zhang, W, R. Piola, A.R., Baques, M., Provost, C., Hernández-Molina, F.J., Felgendreher, M., Spieß, V., Kasten, S. 2021. The erosive power of the Malvinas Current: Influence of bottom currents on morpho-sedimentary features along the northern Argentine margin (SW Atlantic Ocean), Marine Geology 439, https://doi.org/10.1016/j.margeo.2021.106539.

Zalan, P.V. 2005. End members of gravitational fold and thrust belts (GBTFs) in the deep waters of Brazil. In: Shaw, J.H., Connors, C., Suppe, J. (Eds.), Seismic interpretations of contrational fault-related folds, vol. 53. AAPG Memoir, pp. 147–153.

Zouain, R.N.A.,1986. Aspectos da dinâmica sedimentar no Rio de La Plata na porção exterior e na plataforma interna adjacente. Universidade Federal do Rio Grande do Sul, Porto Alegre.

IV. Síntese integradora

IV.1 Conclusões

Este estudo integrado multiescalar e multiproxy acerca de tectônica e sedimentação da Bacia de Pelotas apresentou suas conclusões em dois manuscritos. Cada manuscrito correspondeu ao objetivo geral de entender os controles regionais e suas implicações na deposição da bacia, na forma de objetivos específicos e resultados atingidos em diferentes escalas de trabalho, seguindo um fluxo de análise regional para local.

O Manuscrito 1, “*From the Andes and the Drake Passage to the Rio Grande Submarine Fan: paleoclimatic and paleogeographic evidence in the Cenozoic Era from the South Atlantic – Austral Segment, Pelotas Basin*”, identificou a influência da tectônica da Cordilheira Andina sobre a sedimentação da Bacia de Pelotas na forma de pulsos de soerguimento, bem como identificou a influência climática do alargamento da Passagem de Drake nos depósitos a partir do Oligo-Mioceno através do registro de correntes de contorno. Este estudo, aplicou em sua metodologia interpretação sísmica, backstripping e análise da taxa de espalhamento do Atlântico Sul, utilizando dados públicos de poços e seções sísmicas da Agência Nacional do Petróleo, Gás Natural e Biocombustíveis (ANP) e compilação de chrons presentes na literatura. A integração destas diferentes ferramentas e técnicas de análise com o conhecimento prévio da Bacia de Pelotas e da geologia regional do sul da América do Sul publicado por autores anteriores mostrou os efeitos que eventos tectônicos, climáticos e mudanças paleogeográficas deixaram no preenchimento da Bacia de Pelotas. A Bacia de Pelotas registrou três pulsos compressivos ocorridos nos Andes Centrais em torno de 50 Ma, 27 Ma e 2,5 Ma (Ypressiano, no Eoceno Inferior; Oligo-Mioceno e Plioceno) em resposta ao soerguimento do Platô Puna, Cordilheira Leste e Subandes respectivamente. Em um intervalo entre os dois primeiros soerguimentos, por volta de 30 Ma, a bacia registrou uma inundação relacionada a desaceleração da Placa Sul Americana. Os Andes Meridionais, através de pulsos extensionais, contribuíram para o alargamento da Passagem de Drake e isto também deixou registros na Bacia de Pelotas. Em 34 Ma a bacia registrou o evento de glaciação decorrente da expansão da capa de gelo antarctica, a qual foi associada a um dos pulsos de alargamento da Passagem de Drake e consequente intensificação da Corrente Circumpolar Antárctica (CCA). Já em 20 Ma, em decorrência de outro pulso de alargamento da Passagem de Drake, a CCA impulsionou a interação entre a Corrente das Malvinas e a Corrente do Brasil conduzindo à deposição contornítica na região do Cone de Rio Grande. Adicionalmente este estudo identificou a raiz destes eventos como consequência da interação entre as placas tectônicas Sul Americana, Antártica e Nazca.

No Manuscrito 2, "*Overpressure modelling in the Rio Grande Submarine Fan, Pelotas Basin: the case study of a gravitational fold and thrust belt in the South Atlantic Brazilian Margin*", destaca-se a comprovação da existência de sobrepressão no setor da Bacia de Pelotas onde está localizada a feição denominada Cone de Rio Grande. A partir da discussão regional da gênese desta feição no manuscrito anterior, este estudo analisa, caracteriza e discute aspectos específicos. É o caso da existência de sobrepressão, a qual já era especulada na literatura prévia ao explicar o arranjo estrutural complexo decorrente de colapso gravitacional sobre uma superfície de descolamento. Este estudo aplicou em sua metodologia a modelagem 2D de bacia, utilizando horizontes interpretados em seção sísmica e dados de poço da Agência Nacional do Petróleo, Gás Natural e Biocombustíveis (ANP), localizados na região do Cone de Rio Grande para modelar a sobrepressão e temperatura. Adicionalmente à comprovação e caracterização quantitativa inédita das dimensões e intensidade da sobrepressão, foram discutidas as suas causas e sua relação com a superfície de descolamento e consequente colapso gravitacional. A configuração da temperatura e sobrepressão resultantes da modelagem variam de 6°C até 151°C e 0 MPa até 39 Mpa, com uma tendência geral de valores decrescentes para o topo, exceto próximo da zona de descolamento, onde ocorre diminuição abrupta nos valores. As causas da ocorrência de sobrepressão estão associadas a três principais fatores: a) alta taxa de sedimentação, b) espesso pacote de folhelhos subcompactados e c) transformação de esmectita em ilita. Estes fatores foram classificados em alóctones (a e b) e autóctone (c).

IV.2 Impacto e possível continuidade

Os resultados alcançados na tese apresentam relevância multiescalar e contribuem com diferentes áreas de aplicação do conhecimento. O reconhecimento dos controles alóctones regionais possui impacto global, na medida em que trata de eventos tectônicos e climáticos com interferência no Atlântico Sul. Adicionalmente, contribui para o entendimento da dinâmica e evolução de margens passivas. A partir da dinâmica regional compreendida a tese também contribui com a identificação de causas e produtos de fenômenos internos à bacia. A investigação da sobrepressão é relevante para a exploração de hidrocarbonetos bem como para a predição de desastres naturais decorrentes de colapsos gravitacionais. O desenvolvimento da tese contribuiu com novos dados, resultados e discussões inéditas e aprofundou os estudos acerca do preenchimento e compartimentação estrutural da Bacia de Pelotas.

A continuidade deste trabalho está atrelada à disponibilidade de mais dados. A Bacia de Pelotas, ainda enquanto uma bacia de fronteira exploratória, conta com poucos dados se comparada às bacias marginais vizinhas. As pesquisas na Bacia de Pelotas desenvolvidas com dados públicos da ANP contam com um numero reduzido de poços, nenhum cubo sísmico, número reduzido de seções sísmicas, dados bioestratigráficos ausentes em alguns poços e gerados há duas décadas.

Neste sentido, salienta-se que a existência ou continuidade de um trabalho capaz de trazer avanços para a Bacia de Pelotas, bem como interpretações inovadores e com impacto para a geologia regional, tal como fez a presente tese, está atrelada a geração de novos dados. Para tanto são necessários projetos robustos com o objetivo de enriquecer a base de dados multiescalar e multeferramental da Bacia de Pelotas.

Referências

Abreu, V.S.,1998. Geologic Evolution of conjugate volcanic passive margins: Pelotas Basin (Brazil) and offshore Namibia (Africa) Implication for global sea-level changes. Rice University, Houston.

Abreu, V.S., Anderson, J.B., 1998. Glacial eustasy during the Cenozoic: sequence stratigraphic implications. AAPG Bulletin 82, n. 7, 1385-1400.

Anjos-Zerfass, G.S., 2009. Estudos paleoambientais com base em isótopos de carbono, oxigênio e estrôncio em foraminíferos do Terciário da Bacia de Pelotas. Universidade Federal do Rio Grande do Sul, Porto Alegre.

Bueno. G.V., Zacharias, A.A., Oreiro, S.G., Cupertino, J.A., Falkenhein, F.U.H., Neto, M.A., 2007. Bacia de Pelotas. Boletim de Geociências da Petrobrás 15, n. 2, 557-559.

Chemale Junior, F., Lavina, E.L.C., Carassai, J.J., Girelli, T.J., Lana, C., 2021. Andean orogenic signature in the Quaternary sandy barriers of Southernmost Brazilian Passive margin – Paradigm as a source area. Geoscience Frontiers 12(4),101119. https://doi.org/10.1016/j.gsf.2020.11.015

Fontana, R.L., 1996. Geotectônica e sismoestratigrafia da Bacia de Pelotas e Plataforma de Florianópolis. Doctorate thesis, Universidade Federal do Rio Grande do Sul, Porto Alegre, 216 p..

Gee, J. S and Kent, D. V., 2007. Source of oceanic magnetic anomalies and the geomagnetic polarity time scale. Treatise on Geophysics, vol. 5: Geomagnetism, Elsevier, Amsterdam, pp. 455-507. https://doi.org/10.1016/B978-044452748-6.00097-3

Ketzer et al. (2020).

Koutsoukos, E.A.M., 1982. Geohistória e paleoecologia das bacias marginais de Florianópolis e Santos. Congresso Brasileiro de Geologia 32, 2369-2382.

Lee, E.Y., Wagreich, M., 2018. Basin modelling with a MatLab-based program, BasinVis 2.0: A case study on the Southern Vienna Basin, Austria. Journal of the Geological Society of Korea 54 n. 6, 615-630.

Lee, E. Y., Novotny, J., Wagreich, M., 2019. Subsidence Analysis and Visualization for Sedimentary Basin Analysis and Modelling. Springer. SpringerBriefs in Petroleum

Geoscience & Engineering. Cham, Switzerland. 56 pp. https://doi.org/10.1007/978-3-319-76424-5

Müller R.D., Seton, M., Zahirovic, S., Williams, S.E., Matthews, K.J., Wright, N.M., Shephard, G.E., Maloney, K.T., Barnett-Moore, N., Hosseinpour, M., Bower, D.J., Cannon, J., 2016. Ocean basin evolution and global-scale plate reorganization events since Pangea breakup, Annual Review of Earth and Planetary Sciences, Vol 44, 107-138. DOI: 10.1146/annurev-earth-060115-012211.

Perez-Diaz, L. and Eagles, G., 2014. Constraining South Atlantic Growth with Seafloor Spreading Data. Tectonics 33, 1848-1873. https://doi.org/10.1002/2014TC003644

Perez-Diaz, L., Eagles, G., 2017. A new high-resolution seafloor age grid for the South Atlantic. Geochemistry, Geophysics, Geosystems 18 (1), 457-470.

Rosa, A.P., 2007. Interpretação sismo-estratigráfica da porção da Bacia de Pelotas que engloba o Cone de Rio Grande e a avaliação do seu potencial petrolífero. Universidade Estadual do Norte Fluminense, Macaé.

Stica, J.M., Zalán, P.V., Ferrari, A.L., 2014. The evolution of rifting on the volcanic margin of the Pelotas Basin and the contextualization of the Paraná-Etendeka LIP in the separation of Gondwana in the South Atlantic. Marine and Petroleum Geology 50, 1-21.